STRUCTURE AND ELEVATED TEMPERATURE PROPERTIES OF FERRITIC ALLOYS STRENGTHENED BY INTERMETALLIC COMPOUNDS

Table of Contents

STRUCTURE AND ELEVATED TEMPERATURE PROPERTIES OF FERRITIC ALLOYS STRENGTHENED BY INTERMETALLIC COMPOUNDS

Mangalore Dilip Bhandarkar

Inorganic Materials Research Division, Lawrence Berkeley Laboratory and
Department of Materials Science and Engineering, College of Engineering;
University of California, Berkeley, California

ABSTRACT

A Laves phase of iron and tantalum was utilized to obtain good room and elevated temperature properties in iron based, non-carbon-containing, body centered cubic alloys containing 1 at. pct. Ta and up to 7 at. pct. Cr. The room temperature embrittlement resulting from the heterogeneous precipitation of the Laves phase at grain boundaries and other preferred sites was overcome by the use of an allotropic phase change to spheroidize the precipitate. The microstructure of spheroidized Fe-Ta-Cr alloys was characterized by a uniform distribution of almost spherical particles of the Laves phase in a matrix with irregular grain boundaries. The dislocation substructure of spheroidized Fe-Ta-Cr alloys consisted of subgrains and tangled networks. A high density of dislocations, which were not in all cases pinned by precipitate particles, was present in the alloys. Short-time yield and ultimate tensile strengths of Fe-Ta-Cr alloys decreased very slowly with increase in test temperature upto 600°C, but showed a considerable drop at higher temperatures. Short-time tensile properties were not very sensitive to changes in heat treating procedure. Results of constant load creep and stress rupture tests conducted at several temperatures and stresses indicated that the rupture and creep strengths of spheroidized alloy Ta7Cr (1 at. pct. Ta, 7 at. pct. Cr) were higher than those of several commercial ferritic steels containing dispersions of chromium and/or molybdenum carbides, but lower than those of ferritic steels containing significant amounts of refractory metals such as tungsten and vanadium. Transmission electron microscope studies of the substructure of crept specimens indicated that partial recovery of the original substructure and additional precipitation of the Laves phase occurred during creep at 1100°F (593°C) and 1200°F (649°C). The substructure was characterized by well developed subgrains, a low dislocation density, jogged dislocations, dislocation pile-ups at precipitate particles, and considerable pinning of subgrain boundaries and dislocations by the precipitate particles that were originally present, and the particles that precipitated homogeneously during creep. Structural observations, measured apparent activation energy for creep, and estimated stress sensitivity of steady state creep rates suggested that creep of alloy Ta7Cr was a multistep process with two or more independent mechanisms in parallel. Fracture surface observations of specimens tested at several constant loads and temperatures indicated that fracture was initiated by void formation and growth around precipitate particles. At 1200°F (649°C) void formation and growth occurred preferentially around particles at grain boundaries resulting in intergranular initiation of cracks. The information gained from the investigations on Fe-Ta-Cr alloys was supplemented by information available in the literature to develop a Fe-Ta-Cr-Mo alloy. The rupture and creep strengths of alloy Ta7CrMo with 1 at. pct. Ta, 7 at. pct. Cr, and 0.5 at. pct. Mo were considerably higher than the rupture and creep strengths of alloy Ta7Cr.

I. INTRODUCTION

In recent years, a steady upward trend in the temperature of operation of equipment in petroleum refineries, power generation equipment, aircraft engine components, and similar applications has called for the development of heat-resistant alloys that can withstand ever increasing temperatures. In the past, the development of such materials has been an empirical process based on trial-and-error, and involving the making and testing of hundreds of alloy compositions. This approach is no longer feasible because the complexity of material requirements in modern technology make the approach too uneconomical and time-consuming to be practicable. Therefore, an alloy design approach is needed that involves an application of the basic principles of materials science, maximum use of information available in the literature, and minimum cost of material preparation and testing.

Most commercially available creep resistant materials derive their strength from a uniform dispersion of a second phase which hinders the movement of dislocations. In addition, particles of the dispersed phase retard recovery, probably by anchoring the tangled networks of dislocations which are either originally present, or are produced as a result of creep deformation. In creep resistant ferritic steels, the dispersion almost invariably consists of one or more types of carbides, whereas in high nickel content superalloys, a large volume fraction of the dispersed phase is an intermetallic compound, such as $Ni_3(Al,Ti)$. The particle size, morphology, distribution and volume fraction of the second phase, the degree of its coherency with the matrix, and the mechanical properties of the matrix all affect the creep resistance of dispersion strengthened alloys. The thermal stability of the second phase, and of matrix structure are additional factors that have a significant influence on elevated temperature creep resistance.[1]

The composition, morphology and crystal structure of carbides tend to change slowly at elevated temperatures and this often results in an increase in creep rate. One example of this is found in the case of 0.1C-1Cr-0.5Mo steel. The commonly used heat treatment for this steel results in a dispersion of M_3C type carbide. On long time exposure to an elevated temperature, the carbides M_7C_3 and Mo_2C develop gradually with the eventual formation of M_6C which causes a considerable decrease in creep resistance.[2]

Another problem that is frequently encountered in elevated temperature steels arises from the need to design for oxidation resistance. Chromium additions are usually employed for this purpose. In steels, increasing chromium additions favor the formation of carbides M_7C_3 and $M_{23}C_6$.[3] Neither of these carbides imparts appreciable strengthening at elevated temperatures.[3-5] In addition, the carbide M_7C_3 has a high coarsening rate which further reduces creep resistance.[3-5] Colbeck and Rait[3] found a continuous decrease in the creep strength of chromium-vanadium steels as the chromium content was increased from 1 to 8 pct. On the other hand, worthwhile improvements in oxidation resistance at 600°C are not obtained in ferritic steels until about 7 pct. chromium is present.[4,5] Such alloys, therefore, have inherently low creep strength due to the presence of the carbide M_7C_3. Other attendant problems in ferritic steels are graphitization and temper embrittlement. It is apparent from the above discussion that the several problems that are encountered in the use of ferritic steels for elevated temperature applications are caused by the presence of carbides. Therefore, it would be desirable to eliminate carbides from these steels and devise alternative means of enhancing elevated temperature creep strength. The use of intermetallic compounds is an obvious possibility since several of these compounds are very stable as indicated by their high melting points, and are known for their strengthening effects in iron when present as dispersions.[6]

The concept of using intermetallic compounds, rather than carbides, for enhancing elevated temperature strength is decades old, but progress towards a realization of this concept has been slow. The status of such work was summarized recently by Decker in his paper on nickel-base superalloys.[7] The compound $Ni_3(Al,Ti)$ plays an important strengthening role in these alloys, but carbon in amounts ranging from 0.05 to 0.15 pct. is considered to be essential for high temperature strength. Experiments in which carbon was reduced to very low levels in superalloys resulted in "...sharply reduced creep life and ductility...."[7] This was a rather surprising conclusion since it is known that the carbides that form in superalloys very frequently nucleate at grain boundaries.[7]

In general, intermetallic compounds are more resistant to growth than carbides because their growth requires diffusion of substitutional alloying atoms through the matrix whereas carbides can undergo changes in size, composition and morphology by the interstial diffusion of carbon, in addition to the diffusion of carbide forming alloying elements. A primary difficulty in the elimination of carbides and the use of intermetallic compounds has been the tendency of the latter to precipitate heterogeneously at grain boundaries and other preferred sites, which leads to severe room temperature embrittlement. The effect of intermetallic compounds such as the sigma phase have been reported by Decker and Floreen,[6] Decker[7] and Mihalisin, et al.[8] There was general agreement that the presence of sigma phase lowered both stress-rupture strength and room temperature ductility. Decker[7] also summarized the status of knowledge about the effects of the Laves phase in superalloys. He concluded that in general, when the Laves phase is present in significant amounts, it "…. can degrade room temperature ductility with little effect on creep properties." A similar conclusion has been made on the effect of the Laves phase in ferritic alloys.[9] The results from the present investigation showed, however, that with microstructural control, satisfactory values of room temperature strength and ductility, as well as good creep and rupture strength, could be attained in very low carbon iron alloys strengthened with the Laves phase Fe_2Ta. Some of these results were reported in an earlier paper.[10]

Recently it was demonstrated by Jones, et al.[11] that the brittleness due to the presence of a continuous grain boundary network of the Laves phase Fe_2Ta in binary Fe-Ta alloys was overcome by the use of a simple heat treatment leading to spheroidization of the precipitate phase at the grain boundaries and within the grains. Spheroidization of the Laves phase resulted in considerable enhancement of room temperature ductility and elevated temperature strength of Fe-Ta alloys. Subsequent investigations of Fe-Ta alloys containing various amounts of chromium indicated that the phase transformations and structural features of Fe-Ta-Cr alloys were similar to those of binary Fe-Ta alloys.[12]

One objective of the present investigation was to develop elevated temperature alloys using a dispersion of the Laves phase in a non-carbon-containing body centered cubic iron matrix. An understanding and application of basic principles of materials science and the use of large amounts of information available in the literature were instrumental in the development of Fe-Ta-Cr alloys of the present investigation. The phase transformations that occurred in the alloys, and the resulting microstructures were studied. A second objective was to examine the relation between mechanical properties and structure. Short time tensile mechanical properties and long time creep and stress rupture tests were conducted on the alloys in which microstructural features were varied by changes in the heat treating procedure. The mechanical properties were compared with those of several commercially available steels.

An examination of substructure and precipitate distribution of the alloys before and after creep tests, the determination of apparent activation energy for creep and an estimation of the stress sensitivity of steady state creep rates were carried out in order to investigate the mechanism of creep in dispersion-hardened ferritic alloys. Fracture surface morphology was examined after specimens were tested in short time tension and in creep. The large amount of information obtained on the behavior of alloys of the present investigation is believed to be beneficial for the development of other iron alloys using intermetallic compounds, rather than carbides, for attaining elevated temperature strength.

II. EXPERIMENTAL PROCEDURE

A. Alloy Preparation and Processing

The alloys in the present investigation were prepared using high purity raw materials. The iron used was Glidden A-104 electrolytic iron with a purity of 99.94 pct. Electrolytically deposited chromium with a purity of 99.95 pct. was used. Tantalum and molybdenum rods of 99.9 pct. initial purity were given three pass zone refining treatments prior to use. Heats of approximately 20 lbs were induction melted in an argon atmosphere, cast in heavy copper molds and subsequently annealed in vacuum for 3 days at 1100°C. The chemical compositions of the alloys are listed in Table I.

The ingots were forged at 1100°C into plates 3 in. by 9/16 in. cross section. Creep specimen blanks 9/16 in. by 9/16 in. in cross section and 3 5/8 in. long were cut out of these plates. For tensile specimen blanks the 9/16 in. thick plates were further reduced by rolling at 1000°C to a thickness of 7/32 in., and blanks 7/32 in. by 5/8 in. in cross section and 2 7/8 in. long were cut out.

B. Heat Treatment

Specimen blanks were surface ground to remove the oxide layer and encapsulated in quartz tubes which were previously evacuated and backfilled with argon. The heat treating procedure consisted of one hour solution treatment followed by hot water quenching, aging followed by air cooling and spheroidizing followed by air cooling. The complete heat treating procedure is schematically sketched in Fig. 1 for alloys Ta5Cr and Ta7Cr. The alloy Ta7CrMo was also heat treated in the same manner except for the difference that the solution treating temperature was 1350°C. A molten bath at 700°C was used for aging the specimen blanks. Protective stainless steel bags were used to enclose the blanks during the spheroidizing treatment.

Investigations of structure and mechanical properties were carried out for several variations in the heat treating procedure shown in Fig. 1. The variations consisted of changes in the time and temperature of the spheroidizing treatment, and also the addition of cold working treatments before aging and after spheroidizing. The several different heat treatments are described in Table II.

C. Short-Time Tensile Testing

Sheet tensile specimens of one inch gage length, a thickness of 0.2 in., and a test section width of 0.125 in. were ground from the heat treated specimen blanks. A sketch of the specimen is shown in Fig. 2. The specimens were loaded through aligning pins in the wide ends of the specimens. Tensile tests at temperatures from 22°C to 700°C were carried out using an Instron. The strain rate employed was 0.04 per minute. For the elevated temperature tests, the Instron was outfitted with a controlled atmosphere chamber surrounded by a three-zone resistance furnace. Power inputs to the three zones were independently controlled. Specimen temperature was measured by three thermocouples attached to the specimen, one at each end of the gage section and one in the middle of the gage length. A temperature gradient of less than

2°C was attained along the specimen gage section by proper control of the currents in the three zones. All elevated temperature tests were carried out in an argon atmosphere. The total elongation was measured between two fine scratch marks, one at each end of the gage length. The yield strength was obtained by the 0.2% offset method. Prior to loading, the specimens were held at the test temperature for one hour to insure uniformity of temperature in the gage section.

D. Creep and Stress Rupture Testing

Constant load creep and stress rupture tests were carried out on round specimens with threaded ends and a gage section diameter of 0.25 in. A sketch of the specimen is shown in Fig. 3. A 0.357 in. diameter shoulder was provided between each end of the gage section and the threaded grip portion. A pair of diametrically opposite 1/16 in. deep drills on each shoulder facilitated the use of an extensometer. The extensometer was fitted with dial gages graduated in 10^{-4} in. for measurement of extension. The specimen and extensometer assembly is shown in Fig. 4. The assembly formed a part of the specimen train in the SATEC Model M-3 creep tester fitted with a Model F6-1 furnace and a reactor-type current proportioning system for temperature control. The load was applied by means of a lever arm with a 16:1 ratio. A mercury switch facilitated automatic leveling of the lever arm so that an axial load with minimum eccentricity was maintained during the entire test. Specimen temperature was measured by two thermocouples, one attached to each end of the specimen gage section. The temperature gradient along the gage section was less than 3°C.

Prior to loading, specimens were soaked for one hour at the test temperature. Creep strains, rupture times and steady state creep rates were determined from each test.

E. Structural Analysis

Specimens for optical metallography were prepared by mechanical grinding and polishing followed by chemical etching. The etching solution used was Kalling's Reagent containing 5 gm. of $CuCl_2$, 100 ml of HCl, 100 ml. of ethyl alcohol and 100 ml. of water. Specimens for X-ray analysis were prepared by mechanical grinding followed by chemical polishing to remove the deformed layer resulting from mechanical grinding. A solution containing a 1:1 mixture of H_3PO_4 and H_2O_2 and a few drops of HF was used for chemical polishing. The specimens were examined in a Norelco X-ray diffractometer using CuK_α radiation and a crystal monochromator to reduce the fluorescent radiation.

F. Microhardness Measurements

Measurements of Vickers microhardness were made on metallographically polished and etched specimens using a diamond pyramid indentor and a load of 2 kg. At least five measurements were made on each specimen and an average was taken.

G. Transmission Electron Microscopy

Thin foils for transmission electron microscopy were prepared by the twin jet electropolishing technique using a solution containing 20 pct. perchloric acid and 80 pct. acetic acid. Prior to electropolishing, 0.020 in. thick slices of the material were chemically thinned to 0.003 in. in a solution containing 6 pct. hydrofluoric acid and 94 pct. hydrogen peroxide. Siemens-I and Hitachi HU-125 microscopes, operated at 100 kV, were used for examination of thin foils.

Precipitate distributions were studied also by transmission electron microscopy of carbon replicas. Specimens for replication were metallographically polished, etched and cleaned with extreme precautions to insure a clean and scratch-free surface with minimum deformation. Carbon was deposited in a vacuum evaporator, a grid was scribed in the carbon layer and replicas were extracted by chemically dissolving the base metal. A solution containing 10 pct. HCl in ethyl alcohol was used for extraction. The replicas were rinsed in three stages, first in ethyl alcohol, then in a 1:1 mixture of ethyl alcohol and water, and finally, in water. They were picked up on 200-mesh copper grids and dried before examination in the electron microscope.

H. Scanning Electron Microscopy

Fracture surfaces of short-time tensile specimens and of creep specimens were examined in the JEOLCO JSM-U3 scanning electron microscope operated at 25 kV. Fracture studies in the scanning electron microscope were supplemented by optical metallography of longitudinal sections of test specimens near and away from the fractured ends. The longitudinal sections were taken close to the specimen axis and were ground, polished and etched for metallographic examination.

III. ALLOY DEVELOPMENT

A. The Fe-Ta System

The iron-rich portion of the Fe-Ta binary phase diagram, which has been accurately determined by Sinha and Hume-Rothery[13] is shown in Fig. 5. On the iron-rich side, there are three solid solutions of tantalum in iron, namely, the low temperature body centered cubic solid solution α, the intermediate temperature face centered cubic solid solution γ, and the high temperature body centered cubic solid solution δ. The maximum solid solubility of tantalum in iron occurs in the δ phase field, and is 2.8 at.pct. at 1440($\pm$2)°C. The δ phase decomposes eutectoidally at 1239($\pm$3)°C by the reaction,

$$\delta(1.1 \text{ at.pct. Ta}) \rightarrow \gamma(0.5 \text{ at.pct. Ta}) + Fe_2Ta$$

The γ phase reacts peritectoidally with Fe_2Ta at 972($\pm$3)°C by the reaction,

$$\gamma(0.3 \text{ at.pct. Ta}) + Fe_2Ta \rightarrow \alpha(0.6 \text{ at.pct. Ta}) \quad .$$

The solubility of tantalum in α iron decreases with a decrease in temperature from 972°C but the solvus curve has not been determined. The compound Fe_2Ta is a Laves phase with the hexagonal $MgZn_2$(C14) type crystal structure[14] and a melting point of 1775°C.[15] Hansen[15] showed a stoichiometric composition for the Fe-Ta Laves phase, but suggested that it may exist in a range of homogeneity somewhat similar to the Laves phase in the Fe-Nb system.[16] On the basis of his theoretical analysis of phase stability, Brewer[17] predicted that the Laves phase in the Fe-Ta system should be stable over a composition range of 25 to 35 at.pct. Ta.

Lattice parameter data of Jones[18] and Jones, et al.[19] on the compound in equilibrium with the α solid solution indicated that the interplanar spacings of the compound were approximately the same as those of Fe_7Ta_3. Based on the results of X-ray and electron diffraction, Jones, et al.[19] concluded that the Laves phase in the Fe-Ta system was stable over a range of compositions.

B. Precipitation of the Laves Phase in Fe-Ta Alloys

The phase diagram of the Fe-Ta system indicates that if a supersaturated solid solution can be obtained by quenching an elevated temperature solid solution, then it should be possible to attain precipitation hardening by subsequently aging the supersaturated solid solution.

The results of extensive investigations of the precipitation of the Laves phase in Fe-Ta alloys with tantalum contents ranging from 0.5 to 2.5 at. pct. were reported by Jones[18] and Jones, et al.[19] The alloys were solution treated at 1400°C for 1 hour and water quenched prior to aging at 600°C, 700°C and 800°C for several time intervals. The variation of hardness with aging time was characteristic of precipitation hardening. As the aging time was increased, hardness first increased, reached a peak, and then decreased. Peak hardnesses were observed at decreasing aging times with increasing aging temperature. Precipitation occurred in a heterogeneous fashion. An almost continuous grain boundary network of precipitate was observed in the solution treated condition. Precipitation occurred in the grains during aging. The grain boundary precipitate network was not significantly affected by the aging treatment. The aged alloys were extremely brittle due to the large grain size and the grain boundary precipitate network. The room temperature tensile elongation of alloys with 1 and 2 at.pct. Ta was virtually negligible and the fracture surfaces of tensile specimens showed features characteristic of transgranular cleavage initiated by cracks in the grain boundary precipitate network.[19]

C. Enhancement of Ductility in Fe-Ta Alloys

The grain boundary precipitation of the Laves phase in Fe-Ta alloys was spheroidized using an allotropic phase change.[11] When the aged alloys were heated in the (γ + Fe_2Ta) phase field, α solid solution transformed to γ and the Fe_2Ta precipitate at grain boundaries and within the grains spheriodized. In iron alloys containing 1 at.pct. Ta, hot stage experiments in the scanning electron microscope showed that heat treating for 10 minutes in the (γ + Fe_2Ta) phase field resulted in a structure with a uniform dispersion of Fe_2Ta particles, and the grain boundaries of the prior δ structure were no longer readily noticeable. On cooling back to room temperature, γ transformed to α by a transformation believed to be similar to the massive transformation observed in several iron alloys.[20] The microstructure consisted of a uniform dispersion of about 3 vol.pct. of almost spherical particles of Fe_2Ta in a matrix of the α solid solution with irregular grain boundaries. The spheroidizing treatment considerably enhanced the ductility of Fe-Ta alloys (as exhibited by an increase in room temperature tensile elongation and the change in fracture surface morphology from cleavage to dimpled rupture). A room temperature yield strength of 40,800 psi and a fracture elongation of 30 pct. were observed for the Fe-1 at.pct. Ta alloys spheroidized for 10 min. at 1100°C following one hour aging at 700°C. Elevated temperature tensile tests indicated that a large fraction of the room temperature yield strength was retained upto a test temperature of about 600°C. Further increase in test temperature resulted in a sharp decrease in yield strength.

D. Development of Fe-Ta-Cr Alloys

Two major limitations of Fe-Ta alloys with respect to their possible practical utilization for elevated temperature applications were: 1) the high phase transformation temperatures that necessitated high temperature heat treatments, and 2) inadequate oxidation resistance. Preliminary investigations indicated that at 700°C in an oxidizing atmosphere, the weight gain of the Fe-1Ta alloy was about 30 pct. of that of pure iron.[22] The addition of the element chromium was expected to minimize both the above limitations.

An examination of the binary Fe-Cr phase diagram[23] indicated that increasing chromium additions to iron continuously lowered the $\gamma \rightarrow \delta$ phase transformation temperatures. The $\alpha \rightarrow \gamma$ transformation temperature, on the other hand, was lowered by chromium additions up to about 7 pct., but was raised by further additions of chromium. It seemed reasonable to expect that qualitatively, a similar trend would be observed on addition of chromium to Fe-Ta alloys, though the magnitudes of the changes in phase transformation temperatures, and the amounts of chromium additions needed to achieve those changes might be different in the binary Fe-Cr and the ternary Fe-Ta-Cr alloys.

The enhancement of oxidation resistance resulting from chromium additions to iron is a well known phenomenon. Studies of the oxidation behavior of Fe-Cr alloys have indicated that at 1000°C, the weight loss due to oxidation decreases significantly with chromium additions up to about 7 pct., then remains approximately constant till about 12 pct. Cr, and decreases again to very low values at 18 pct. Cr.[24] A similar effect of chromium additions may be expected in Fe-Ta-Cr alloys though the magnitude of the effect may be different from that in binary Fe-Cr alloys.

The factors discussed above led to the development of ternary Fe-Ta-Cr alloys Ta5Cr (1 at.pct. Ta and 5 at.pct. Cr) and Ta7Cr (1 at.pct. Ta and 7 at.pct. Cr). In both alloys, the tantalum content was limited to 1 at.pct., since higher or lower tantalum contents were expected to raise the temperatures needed to attain the single phase δ in the first step of the heat treating cycle shown in Fig. 1. Metallographic studies of specimens of Ta5Cr and Ta7Cr solution treated for one hour at several temperatures and water quenched indicated that a structure with a single phase δ and a grain boundary envelope of the Laves phase was obtained at lower solution treating temperatures in the ternary Ta5Cr and Ta7Cr alloys than in the binary Fe-1Ta alloy. A more detailed study of the tranformation behavior of Fe-Ta-Cr alloys has been reported elsewhere.[12] The present investigation was mostly confined to the structure and elevated temperature properties of Ta5Cr and Ta7Cr alloys and their subsequent modifications involving alloying additions of molybdenum.

IV. RESULTS AND DISCUSSION

A. Phase Transformations and Microstructures of Fe-Ta-Cr Alloys

As mentioned in an earlier section, increasing chromium contents up to 7 at. pct. lowered the phase transformation temperatures in alloys of iron containing 1 at. pct. tantalum. The temperature to attain single phase δ was lowered by 60°C with addition of 5 at.pct. Cr to Fe-1 at.pct. Ta alloy, and by 90°C with addition of 7 at.pct. Cr. In subsequent investigations, one hour solution treatment at 1320°C was employed for both Ta5Cr and Ta7Cr alloys. The solution treated samples were quenched in hot water. The microstructures of solution treated and quenched alloys were characterized by large grains (approximately 1 mm in average diameter) an an almost continuous grain boundary network of precipitate. When the solution treated alloys were aged at an elevated temperature, additional precipitate formed within the grains, and there was no noticeable change in the grain boundary network of precipitate. Microhardness measurements on samples aged for several time intervals at 700°C showed that the hardness first increased with increasing aging time, reached a maximum, and then decreased. Time to attain peak hardness was 40 min. for both Ta5Cr and Ta7Cr aged at 700°C. The variation of hardness with aging time at 700°C is shown in Fig. 6 for the Ta7Cr alloy. The microstructure of the alloy in the peak hardness condition is shown in Fig. 7.

In Fig. 8 is shown the transmission electron micrograph of a carbon extraction replica from a peak aged specimen of alloy Ta7Cr. The precipitate particles were mostly rod shaped, though some almost spherical particles were also observed. Relatively long lines of precipitate particles were frequently observed. These were attributed to preferred nucleation of precipitates on dislocations. Transmission electron microscopy of thin foils of similar alloys showed that the precipitate first formed coherently, then lost its coherency by the formation of ⟨100⟩ type dislocation loops, which, in turn, acted as sites for preferred nucleation and growth of precipitates during subsequent aging.[25]

X-ray diffractometer studies made on specimens of alloy Ta7Cr, aged for 40 hrs. at 700°C, indicated that the interplanar spacings of the precipitate were very nearly those of Fe_7Ta_3. The stoichiometric composition of Fe_7Ta_3 is within the range of compositions (25 to 35 at. pct.) predicted by Brewer[17] for the Laves phase in Fe-Ta alloys. In discussions that follow, the precipitate in the alloys of the current investigation is referred to as the Laves phase, or as Fe_2Ta, the stoichiometric composition of which is the basis for the Laves phase.

When the aged alloys were heated to 1100°C, the matrix transformed to the face centered cubic solid solution γ, and both the grain boundary precipitate and the precipitate within the grains spheroidized. On cooling from the γ phase field, the matrix transformed to α, with a refinement of the grain size. The microstructure of alloy Ta7Cr after a 10 min. spheroidizing treatment at 1100°C followed by air cooling is shown in Fig. 9. The structure was characterized by a fine distribution of the Laves phase in a matrix of α grains with irregular boundaries. The irregular grain boundaries resulted from the transformation of

γ to α during cooling from 1100°C. The transformation was believed to be similar to the massive transformation that has been observed in several iron-base alloys.[21] In subsequent investigations on similar alloys, it was shown that the transformation of $\alpha \rightarrow \gamma$ on heating was time and temperature dependent, and these studies are reported elsewhere.[25]

Transmission electron micrograph of a carbon extraction replica taken from a specimen of alloy Ta7Cr spheroidized at 1100°C for 10 min. is shown in Fig. 10. It was evident that after the spheroidizing treatment the precipitate particles in the alloy were almost spherical and formed a homogeneous distribution. Particle sizes ranging from about 0.03 μ to about 0.3 μ were observed.

Transmission electron micrograph of a thin foil specimen of alloy Ta7Cr, spheroidized at 1100°C for 10 min. following solution treating and aging (Heat Treatment T-1), is shown in Fig. 11. The alloy exhibited a lath-like structure similar to that observed in several low carbon or non-carbon-containing iron-based alloys which undergo a massive transformation from austenite to ferrite.[21,26] The substructure within the laths was characterized by a high dislocation density. In Fig. 12(a) is shown a high magnification bright field micrograph of the same alloy. A lath boundary is indicated by ABCDEFG. The selected area that is outlined by the image of the aperture in Fig. 12(a) gave two superimposed single crystal patterns. The bright field image was obtained after tilting the specimen to get a two-beam diffracting condition in the lath above the boundary CD. The operating g-vector was $[01\bar{1}]$ as shown in Fig. 12(a). The dislocation substructure consisted of tangled networks (as in the area around P) and a cell-like structure with high density of dislocations at cell walls (at O). In Fig. 12(b) is shown the bright field image of the area in Fig. 12(a) when the operating g-vector was $[0\bar{3}1]$. A cell-like structure is evident in the area R in Fig. 12(b). In Fig. 13(a) is shown a bright field micrograph from another area of the foil which again illustrates the several substructural features discussed above. Dislocation networks (at P) and the lath-like structure are clearly observed in Fig. 13(a). A diffraction pattern taken from the selected area imaged in the bright field micrograph of Fig. 13(a) is shown in Fig. 13(b). The boundary AB in Fig. 13(a) was a high angle boundary and accordingly the diffraction pattern consisted of two superimposed single crystal patterns, with reflections denoted by 1, 2 and 3 belonging to one pattern, and 4 and 5 belonging to the other. On careful observation the matrix spot 3 was resolved into two closely spaced matrix spots indicating that in the cell-like substructure discussed earlier, the cell boundaries were low angle boundaries.

An examination of Fig. 11 indicated that precipitate particles were almost spherical and were uniformly distributed. This observation supported the conclusion made earlier in this section from an examination of the precipite distribution in carbon extraction replicas (Fig. 10). As was the case in Fig. 10, precipitate particles ranging in diameter from 0.03 μ to 0.3 μ were observed in Figs. 11, 12 and 13. It was shown later that fracture surfaces of tensile and creep specimens contained particles of size as high as 4 μ.

In short, the matrix of alloy Ta7Cr heat treated by process T-1 was best described as consisting of ferritic laths with a high dislocation density in the form of tangled networks and subgrains with low angle boundaries. The laths themselves were separated by high angle boundaries in some cases and low angle boundaries in other cases. Similar structures have been observed by other investigators in other low carbon iron alloys.[26] The precipitate particles in alloy Ta7Cr ranged in diameter from about 0.03 μ to about 4 μ and were uniformly distributed. Particle-dislocation interactions were observed in some areas where the dislocation substructure was pinned by the precipitate particles. Examples of this can be seen in Figs. 12 and 13. However, there was a high density of unpinned dislocations.

B. Short-Time Tensile Properties of Fe-Ta-Cr Alloys in the Aged Condition, Before Spheroidizing

The short-time yield strength, ultimate tensile strength and percent elongation at fracture of alloy Ta7Cr aged at 700°C for 40 min. are listed in Table III and plotted in Fig. 14 as a function of test temperature. Both the yield and ultimate strengths decreased as the test temperature increased. The decrease in strength was gradual up to a test temperature of about 600°C; at this temperature the yield strength was about 70 pct. of the room temperature value and the ultimate tensile strength was about 48 pct. of the room temperature value. Both the yield and ultimate tensile strengths decreased more rapidly as the test temperature increased. Also associated with the increase in test temperature was a decrease in the difference between the ultimate tensile strength and the yield strength. From these observations it was evident that the strain hardening rate decreased with increase in test temperature. Scanning electron fractographs of tensile specimens of the alloy Ta7Cr, aged at 700°C for 40 min., tested at various temperatures are shown in Fig. 15. The fracture surface of the specimen tested at 22°C [Fig. 15(a)] was characterized by flat areas, steps, and river markings which are typical cleavage features. Fracture was apparently initiated at the grain boundary precipitate envelope and propagated in a transgranular manner. Fracture surfaces of specimens tested at 200°C [Fig. 15(b)], 400°C [Fig. 15(c)] and 600°C [Fig. 15(d)] indicated increasingly ductile behavior, and fracture was characterized by predominantly cleavage and quasi-cleavage at 200°C, quasi-cleavage and dimpled rupture at 400°C, and predominantly dimpled rupture at 600°C. A large portion of the dimpled rupture observed at 600°C was initiated by void formation at precipitate-matrix interfaces (Fig. 15(d)). Figure 15(d) also shows dimples formed by extensive ductile tearing. Void formation and ductile tearing resulted in a fracture appearance characterized by a wide range of dimple sizes.

C. Short-Time Tensile Properties of Spheroidized Fe-Ta-Cr Alloys

The room temperature fracture behavior was changed from brittle to ductile by the spheroidizing treatment that followed aging. The scanning electron fractograph of the tensile specimen of alloy Ta7Cr spheroidized at 1100°C for 10 min., and tested at 22°C is shown in Fig. 16(a). These was evidence of a significant amount of plastic deformation as indicated by dimpled rupture. Dimple formation was almost entirely initiated by void formation at precipitate-matrix interfaces. Typically there were large dimples of sizes ranging from 10 to 25 μ separated by areas with smaller dimples of sizes 1 μ or less. Precipitate particles as large as 4 μ were observed in the larger dimples. Void formation was initiated apparently at these larger precipitate particles, and plastic flow resulted in the growth of the voids to a stage when final failure resulted by failure resulted by failure of the areas between the large voids. In Fig. 16(b) is shown the scanning electron fractograph of the tensile specimen of the Ta7Cr alloy, aged at 700°C for 40 min, and tested at 22°C. The change in the fracture behavior that results due to the spheroidizing treatment is clearly evident from a comparison of Fig. 16(a) and (b). The short-time tensile properties of alloy Ta7Cr spheroidized at 1100°C for 10 min. after aging at 700°C for 40 min are listed in Table IV and plotted in Fig. 17 as a function of test temperature. Yield and ultimate tensile strengths, and fracture elongation of the spheroidized Ta7Cr alloy were higher than those observed for the same alloy in the aged condition. The increase in fracture elongation was attributed to the change in precipitate morphology and distribution resulting from the spheroidizing treatment. The higher strength levels were attributed to a refinement of the grain size due to the $\alpha \rightarrow \gamma \rightarrow \alpha$ phase change cycle that accompanied the spheroidizing treatment (from about 1 mm in the aged condition to about 200 μ in the spheroidized condition) and the increased dislocation density in the spheroidized alloys. As reported in an earlier section, examination of thin foils of specimens of alloy Ta7Cr spheroidized at 1100°C for 10 min. showed a high dislocation density substructure that consisted of subgrains and dislocation tangles.

D. Effect of Variations in the Heat Treating Procedure on the Short-Time Tensile Properties of Fe-Ta-Cr Alloys

The mechanical properties of dispersion hardened alloys are normally influenced by variables pertaining to the dispersion such as particle size, interparticle spacing, nature of the distribution, and the degree of coherency of the particles with the matrix. In the Fe-Ta-Cr alloys of the present investigation, changes in heat treating procedure were expected to change one or more of the factors listed above. The effect of heat treating procedure on short-time tensile properties was investigated for alloy Ta7Cr. In Table II several heat treating procedures are described, and their designations are listed. The influence on the dispersion was expected to be different for the several different heat treating procedures. As an example, other investigators[27,28] have shown that cold working prior to aging increases the number of nucleation sites, and the precipitate dispersion attained on subsequent aging a consists of finer and more closely spaced particles than is the case without cold work. The results of short time tensile tests at elevated temperatures are listed in Tables V, VI and VII for alloy Ta7Cr heat treated according to the procedures designated as T-1, T-2, T-3 and T-4 in Table II. Also shown in the Tables V-VII are the short-time tensile properties of spheroidized Fe-Ta alloy,[11] of alloy Ta7Cr after heat treatment T-0, and of alloy Ta5Cr after treatment T-1. The differences in short-time tensile properties resulting from the differences in heat treatments T-1, T-2, T-3 and T-4 were small in the case of the Ta7Cr alloy. In Fig. 18, the yield strength of alloy Ta7Cr is plotted as a function of test temperature for the heat treatments T-1, T-2, T-3 and T-4. It can be seen from Fig. 18 that the yield strength data were within a narrow band, the width of which continuously decreased at test temperatures above about 500°C. At 700°C, the yield strengths were virtually the same for the different heat treatments, and the value was the same as that for the alloy tested after aging as can be noted from Table V. The precipitate morphology and distribution in the aged alloy were considerably different from those in the spheroidized alloys as stated in an earlier section. The results discussed above indicated that as the test temperature approached 700°C, precipitate distribution and morphology did not have a significant influence on short-time yield strength, and the nature of the matrix itself was more important. As shown elsewhere[25,29] creep resistance in long time tests was considerably affected by precipitate size, distribution and morphology, and matrix characteristics.

The short-time yield strength, at 700°C, of alloys heat treated by several different procedures suggested that in the ferritic alloys of the present investigation, there was a need to enhance matrix strength in such a manner that the enhanced strength would be retained at elevated temperatures. It is well known that matrix strength can be altered either by changing the matrix substructure or by alloying additions. In dispersion hardened alloys with a stable precipitate dispersion it has been shown that precipitate particles serve to maintain elevated temperature strength by stabilizing the dislocation distribution.[30-34] The ability of a dispersion to stabilize the dislocation substructure has been shown to depend on factors such as the precipitate size, morphology, distribution, volume fraction, and stability.[32-34] It was of interest to investigate whether the Laves phase dispersion in the Ta7Cr alloy was effective in stabilizing dislocation networks and thus in enhancing matrix strength at elevated temperatures. The alloy after spheroidizing at 1100°C for 10 min. was cold worked at room temperature to a 20 pct. reduction in thickness (Treatment T-5 listed in Table II). The room temperature yield strength was increased by about 40 pct. by the cold working treatment. The results of elevated temperature tensile tests on the cold worked alloy are listed in Table VIII. Also shown are the elevated temperature tensile properties of the same alloy before the cold working treatment. The yield strengths are plotted as a function of test temperature in Fig. 19 for both the spheroidized (Heat Treatment T-1) and spheroidized and cold worked (Heat Treatment T-5) alloys. It was evident that the yield strength of the cold worked alloy was higher than that of the alloy without cold work, but as the test temperatures was increased, the difference in yield strength between the two decreased. At test temperatures approaching 700°C, the alloys had approximately the same strength. The above results suggested that the dislocation substructure attained by the room temperatures deformation of alloy Ta7Cr was not sufficiently stabilized by the precipitate dispersion, particularly in short-time tests at temperatures close to or higher than 700°C.

F. Stress Rupture Properties of Alloy Ta7Cr

Constant load stress rupture tests were conducted at 900°F (482°C), 1000°F(538°C), 1100°F(593°C), and 1200°F(649°C) on alloy Ta7Cr spheroidized for 10 min. at 1100°C following solution treatment at 1320°C for one hour and aging at 700°C for 40 min (Heat Treatment T-1). The test results are summarized in Table IX. Log-log plots of stress vs. rupture time at 1000°F(538°C) and 1100°F(593°C) are shown in Fig. 20. The relation between log stress and log rupture time was linear at both test temperatures.

It was of interest to examine how the stress rupture properties of alloy Ta7Cr compared with commercially available elevated temperature ferritic steels. Commercially available ferritic steels can be divided into three principal categories: (i) low and medium alloy steels with low (less than 5 pct) chromium contents, (ii) ferritic steels with 5 to 11 pct. chromium, and (iii) ferritic and martensitic stainless steels with chromium contents of 12 pct. or higher.

Steels in each of the above categories have unique properties that are to be considered in selecting the steels for specific applications in service. All the above steels are used in the annealed, normalized, or normalized and tempered condition in which they consist of dispersions of one or more carbides in a matrix with varying amounts of tempered martensite, ferrite and pearlite.

Low and medium alloy steels with low chromium contents are used up to about 1100°F(593°C) in applications which demand moderate resistance to corrosion and oxidation. A well known steel in this group is the 0.3C-1Cr-1Mo-0.25V steel. In the normalized and tempered condition this steel contains a dispersion of vanadium carbide (V_4C_3) and cementite (Fe_3C) in a ferritic matrix.[35,36] The excellent elevated temperature stress rupture properties of this steel are attributed to the presence of V_4C_3 which is very stable and resistant to growth.[35] Insufficient oxidation and corrosion resistance, and relatively high creep rates[37] particularly at temperatures higher than 1100°F(593°C) limit the use of this steel.

Steels with low chromium contents are inadequate for long time service above 1100°F, where scaling becomes very severe. It is well known that a marked increase is attained in resistance to oxidation in air and steam when steels with higher chromoum contents are used.[37,38] Intermediate chromium steels containing 5 to 11 pct. chromium were developed to meet oxidation resistance requirements up to temperatures as high as 1500°F(816°C). Two common steels in this group are the 0.15C-7Cr-0.5Mo steel and the 0.15C-9Cr-1Mo steel. The higher chromium contents in these steels result in an increasing tendency to form the chromium carbide Cr_7C_3 and the alloy carbide $M_{23}C_6$.[5] Neither of these carbides is as effective as V_4C_3 in enhancing elevated temperature strength, and as a result, the 0.15C-7Cr-0.5Mo and 0.15C-9Cr-1Mo steels have lower stress rupture properties than those of the best lower chromium steels. However, at temperatures above 1100°F, the higher chromium steels have superior oxidation resistance.

Stainless steels with chromium contents of 12 pct. and higher may be hardenable (martensitic) or non-hardenable (ferritic). AISI types 403, 410 and 422, and Greek Ascoloy are some of the more commonly used hardenable stainless steels. Their prime characteristics are good resistance to attack by many corrosive media and against oxidation at elevated temperatures. The types 403 and 410 have the highest elevated creep strength among the straight chromium stainless steels (with no alloying additions of nickel or refractory elements). Greek Ascoloy and the type 422 stainless steel belong to the group of stainless steels which are often referred to as the 12 pct. chromium superalloys. They differ from other 12 pct. chromium steels of the AISI 400 series principally in their refractory metal content. The 12 pct. chromium superalloys contain alloying additions of molybdenum, tungsten, vanadium and other refractory metals. These steels have good elevated temperature strength and resistance to oxidation and corrosion. The ability of these steels to retain good creep resistance at high temperatures is attributed mainly to the stability of the carbides that form in them.

The stress rupture properties of alloy Ta7Cr were compared with the properties quoted in the literature[37] for typical steels in the three categories described above. The results at 1000°F(538°C) and 1100°F(593°C) are shown in Fig. 21 and Fig. 22 respectively. It was observed that at both test temperatures, the stress rupture properties of alloy Ta7Cr were lower than those of 0.3C-1Cr-1Mo-0.25V steel, type

422 stainless steel and Greek Ascoloy, but were higher than those of 0.15C-9Cr-1Mo steel, 0.15C-7Cr-0.5Mo steel and types 403 and 410 stainless steels. The 1000 hour rupture stress at 1100°F(593°C) is listed for alloy Ta7Cr and several other steels in Table X. From the above results it was apparent that the stress rupture properties of alloy Ta7Cr were higher than those of steels of chromium contents between 5 and 12 pct. when the dispersion present in those steels consisted only of carbides of chromium and molybdenum. Rupture strength of steels containing significant volume fractions of carbides of elements such as vanadium and tungsten was much higher than that of alloy Ta7Cr.

Further improvements were attained in the rupture strength of alloy Ta7Cr by modifications in the heat treatment[29] and by alloying additions of molybdenum. The influence of molybdenum additions is discussed in a later section.

F. Creep Rates of Alloy Ta7Cr

Steady state creep rates were determined at various stresses and temperatures for alloy Ta7Cr spheroidized at 1100°C for 10 min (Heat Treatment T-1). The results are shown in Table XI. Steady state creep rates at 1000°F(538°C) and 1100°F(593°C) are plotted against stress on a log-log plot in Fig. 23. A linear relationship was observed at both test temperatures. At constant temperature, the relationship between stress and creep rate was of the form

$$\dot{\varepsilon}_s = A\sigma^n$$

where $\dot{\varepsilon}_s$ is the steady state creep rate, σ is the nominal stress, and A and n are constants. The exponent n, often referred to as the stress sensitivity of steady state creep rates, was independent of test temperature and was approximately equal to 6.5. The value of n in the present investigation was approximately the same as that observed by Amin and Dorn[39] for a dispersion strengthened steel.

A measure of creep strength is provided by the stress required for a creep rate of 1×10^{-4} pct. per hour. The values of the stress for a creep rate of 1×10^{-4} pct. per hour at 1000°F(538°C) and 1100°F(593°C) for alloy Ta7Cr were determined from Fig. 23 by extrapolation. The values of stress for a creep rate of 1×10^{-4} pct. per hour at 1000°F(538°C) are listed in Table XII for alloy Ta7Cr (Heat Treatment T-1) and several commercially available ferritic steels.[37,40] It can be observed from Table XII that the creep strength of alloy Ta7Cr was higher than the creep strength of 0.3C-1Cr-1Mo-0.25V, 0.15C-7Cr-0.5Mo and 0.15C-9Cr-1Mo steels, and types 403 and 410 stainless steels, but lower than that of type 422 stainless steel. Further improvements in creep strength were attained by modifications in the heat treating procedure[29] and by alloying additions of molybdenum as described in a later section.

G. Structural Changes in Alloy Ta7Cr During Creep at 1100°F(593°C)

Thin foils for electron microscopy were prepared from a specimen of alloy Ta7Cr (Heat Treatment T-1) tested to rupture at 1100°F(593°C) and 15,000 psi. The rupture time was 1809 hrs. Foils were taken from the specimen gage section well away from the necked region at the fracture surface. Transmission electron microscopic examination of the foils indicated several structural changes that occurred as a result of exposure to the creep conditions stated above. The bright field micrograph in Fig. 24 shows a distribution of an extremely fine precipitate in addition to the coarser precipitate distribution that was present in the specimen before creep (Figs. 10-13). The finer particles which precipitated on exposure to stress and temperature in the creep tests were mostly of diameters less than 0.03 μ. Another illustration of precipitation that occurred during creep is seen in Fig. 25(a) which shows a micrograph of a foil taken from another area of the same creep specimen. In Fig. 25(b) is shown the diffraction pattern obtained from the selected area enclosed by the image of the aperture in Fig. 25(a). The matrix was in a two-beam diffracting condition with a g-vector of [110]. The reflections A, B and C corresponded to an interplanar spacing of 2.40 Å which was in close agreement with the spacing for the $(11\bar{2}0)$ planes of the Laves phase precipitate that was present in the alloy before creep testing. The dark field micrograph of the reflection B is shown in Fig. 25(c) where several fine precipitate particles reversed contrast. These observations and other measurements of interplanar spacings from electron diffraction patterns showed that the compound that precipitated during creep was the same Laves phase that was originally present in alloy Ta7Cr. An examination of the plot of creep strain vs.time, shown in Fig. 26, did not show any discontinuities in the steady state region. Therefore it was concluded that the precipitation occurred during the tertiary stage of creep. In other alloys, similar precipitations during creep has been found to result in strengthening.[41] In alloy Ta7Cr the precipitation during creep was possibly responsible for a prolonged life in the third stage of creep. The specimen tested at 1100°F(593°C) and 15,000 psi had a total rupture like of 1809 hrs, out of which the third stage of creep alone accounted for about 1400 hrs. as can be noted from Fig. 26. However, it was not possible to conclude that the precipitations during creep prolonged the third stage life by a strengthening effect because the depletion of solid solutions alloying in the matrix and consequent increase in ductility could also lead to a prolonged third stage life.[42]

Examination, by transmission microscopy, of substructure of the specimen crept at 1100°F(593°C) and 15,000 psi revealed that there was a considerable decrease in dislocation density during creep. It was obvious that the lath-like structure that was present before creep underwent recovery during the creep test, and a subgrain structure developed. The boundaries of the subgrains were thinner and less ragged as compared to the boundaries before creep, and were pinned by precipitate particles. The above features are illustrated in Fig. 27. There was evidence of several types of precipitate-dislocation interactions. Both coarse and fine precipitate particles seemed to play an important role in pinning the dislocation substructure. Coarse particles were effective in pinning both individual dislocations and subgrain boundaries, whereas fine particles effectively pinned individual dislocations. Figure 28 shows a bright field image in a two-beam diffracting condition with $[2\bar{1}\bar{1}]$ as the main diffracted beam. The boundaries AB, AC and AD are low angle boundaries. The micrograph shows several dislocation segments that are pinned by coarse precipitate particles (as the segment PQ) and those which are pinned by fine particles precipitated during the creep test (as the segment RS). Similar features are also noted in Fig. 29 which shows a bright field image of the same area as in Fig. 28, but in a two-beam diffracting condition with $\bar{g} = [112]$ as the operating reflection. More illustrations of dislocation pinning by coarse particles are shown in Fig. 30. In Fig. 31 an array of piled up dislocations is indicated at A. Figure 32 shows dislocation segments which give the appearance of jogs (at A, B and C). Jogged dislocations have also been observed by Wilcox and Clauer in Ni-ThO_2 alloys subjected to elevated temperature creep.[33]

H. Structural Changes in Alloy Ta7Cr During Creep at 1200°F (649°C)

Foils taken from a specimen of alloy Ta7Cr (Heat Treatment T-1) tested at 1200°F (649°C) and 11,000 psi were examined in the electron microscope. The rupture time under these creep conditions was 119 hrs. The bright field image shown in Fig. 33(a, indicated that the structure was characterized by a low dislocation density, and consisted of subgrains with relatively regular boundaries. The boundaries were pinned by precipitate particles. The micrograph in Fig. 33(a) was taken after tilting the foil to get a two beam diffracting condition with $\bar{g} = [211]$ as the operating reflection. The diffraction pattern shown in Fig. 33(b) was obtained from the selected area indicated by the image of an aperture in Fig. 33(a). Dislocation pile-ups and dislocations pinned by precipitate particles are indicated at A and B respectively in Fig. 33(a). More examples of dislocation pile-ups are shown in Fig. 34 at A, B and C. In Fig. 35 is shown another illustration of dislocation pinning by precipitate particles (near A). An illustration of pinning of subgrain boundaries by precipitate particles is shown in Fig. 36. A feature that was characteristic of specimens crept at 1200°F (649°C), and which was not observed in specimens crept at 1100°F (593°C) was evidence of deformation at boundaries that were pinned by precipitate particles. Example of this are shown in Fig. 37 at A, B and C. This suggested that these boundaries were tending to move away from precipitate particles possibly by a sliding process which is also a characteristic of elevated temperature creep in TD nickel.[31] This hypothesis was additionally supported by the distorted region at the triple point at D in Fig. 37.

Another important structural feature of the specimen crept at 1200°F (649°C) was the absence of fine precipitate particles that were observed in the specimen crept at 1100°F(593°C). In Fig. 38 are shown structures of alloy Ta7Cr (a) after Heat Treatment T-1, before creep testing, (b) after testing to rupture (1809 hrs.) at 1100°F(593°C) and 15,000 psi, and (c) after testing to rupture (119 hrs) at 1200°F(649°C) and 11,000 psi. A comparison of the three structures indicated differences in the precipitate distributions. On exposure to creep conditions at 1100°F (593°C) there was precipitation of fine particles of the Laves phase while particles originally present before creep were relatively unaltered.

In the specimen exposed to creep at 1200°F (649°C) no fine particles were observed, and the precipitate distribution consisted of a large number of coarse particles. It was concluded that particles precipitated during creep at 1200°F (649°C) coarsened at relatively high rates.

I. Mechanism of Creep in Fe-Ta-Cr Alloys

Over the last decade or two there have been several attempts to develop qualitative and quantitative analyses of the creep behavior of dispersion hardened materials. It seems appropriate to review these theories before any conclusions are arrived at with regard to the mechanism of creep in the Fe-Ta-Cr alloys of the present investigation.

Weertman[43] and Ansell and Weertman[44] proposed a quantitative analysis for creep in coarse grained dispersion hardened materials basing their analysis on the concept that climb, either of single dislocations or of dislocation loops, over particles of the dispersed phase was the rate-controlling step in steady state creep. Under these conditions, the activation energy for creep should be equal to the activation energy for self diffusion in the matrix, and creep rate should vary with stress linearly at low stresses, be proportional to the fourth power of stress at intermediate stresses, and vary exponentially with stress at high stresses. These features are not in agreement with most experimental observations. Some agreement between predicted and observed stress dependence was observed by Ansell and Lenel,[45] but, in general, experimentally observed stress dependence is much higher than that predicted.[31-34,46] In addition, experimentally observed activation energies for creep in dispersion hardened materials are much higher than the activation energies for matrix self-diffusion.[31,44,47,48] The descrepency between predicted and observed activation energies in as-extruded dispersion hardened aluminum alloys was qualitatively explained by Ansell and Weertman on the assumption that in these alloys, the rate-controlling step was the generation of dislocations at grain boundary sources.[44] Ansell and Lenel concluded from their experiments on recrystallized SAP type alloys that dislocation climb was the rate-controlling step and the descrepency between observed and predicted creep rates could be explained if the density of active dislocation sources in the alloys was lower than that assumed in the analysis of Ansell and Weertman.[45] No conclusive structural observations were presented to show the presence or absence of grain boundary dislocaton sources or the density of active dislocation sources.

Wilcox and Clauer[31] studied the creep behavior of thoriated nickel both above and below 0.5 T_m (absolute melting point). At temperatures below 0.5 T_m, they observed elongated dislocation loops attached to ThO_2 particles, and suggested that the loops were formed by cross slip of dislocations around ThO_2 particles leaving prismatic loops around the particles. They concluded that the main mechanism of creep was cross slip of dislocations around dispersed ThO_2 particles. The cross slip mechanism was able to explain the stress dependent activation energies that were observed. However, there was no conclusive evidence to explain the observed stress dependence of creep rate at temperatures below 0.5 T_m. In the same alloys at temperatures above 0.5 T_m, Wilcox and Clauer showed that the major contribution to the plastic creep strain was from grain boundary sliding, but with this mechanism it was not possible to explain the high activation energy and the stress sensitivity of creep rates. Based on their results and those of Takahashi, et al.[49,50] Wilcox and Clauer[33] suggested that the stress sensitivity of creep rates was a structure dependent parameter, and increased as the effective grain size or subgrain size decreased. This idea was extended later to explain the high temperature creep behavior of recrystallized Ni-ThO_2 alloys based on a modified climb mechanism. Sidey and Wilshire[46] attributed the creep resistance of the dispersion hardened alloy Nimonic 80A primarily to the retardation of recovery by particles, and on this basis, qualitatively explained the observed high activation energy for creep and the high stress sensitivity of creep rates. A similar theory has also been proposed by Lagneborg.[51]

Another recent attempt at explaining the high activation energy and stress sensitivity of creep rates in dispersion hardened materials is based on the existence of a stress field arising from the presence of surface tension forces at particle-matrix interfaces.[52] The stress field results in enhancement of creep strength by resisting both glide-controlled and climb-controlled dislocation motion. The presence of surface tension matrix strains at particle-matrix interfaces was, however, not conclusively shown. Moreover, the analysis was based on the assumption that the surface tension force was the same as the surface energy. The validity of this assumption has been questioned.[53]

It is readily evident from the above review that the observed structural features, activation energies for creep and stress sensitivities of creep rates of dispersion hardened materials are not always in agreement with proposed creep models. In the same material, a single model is able to explain only some, but not all, of the experimental observations. It was of interest to examine the applicability of proposed creep models to the spheroidized alloy Ta7Cr of the present investigation.

The discussion of experimental results related to the elevated temperature deformation of alloy Ta7Cr can be broadly divided into two aspects--mechanical testing, and microstructural studies.

With regard to mechanical testing, it was stated in an earlier section that log-log plots of stress vs. steady state creep rates yielded a stress sensitivity exponent of $n = 6.5$, which was slightly higher than the value $n = 4$ to 5 observed for most solid solutions.[54] Apparent activation energy for creep at 1000°F (538°C) was measured by creep testing a single specimen according to the method that has been used by other investigators in the past.[55,56] A constant stress of 25,000 psi was used and the test temperature was cycled from about 985°F (530°C) to about 1015°F (546°C), allowing the specimen to reach steady state at each temperature before the temperature was changed. The apparent activation energy for creep was calculated from the relation,

$$Q_a = \frac{\partial \ln \dot{\varepsilon}_s}{\partial(-\frac{1}{RT})} \simeq \frac{\Delta \ln \dot{\varepsilon}_s}{\Delta(-\frac{1}{RT})} = \frac{R \ln \frac{\dot{\varepsilon}_{s2}}{\dot{\varepsilon}_{s1}}}{\frac{1}{T_1} - \frac{1}{T_2}}$$

where $\dot{\varepsilon}_{s1}$ and $\dot{\varepsilon}_{s2}$ were steady state creep rates at absolute temperatures T_1 and T_2°K respectively and Q_a was the apparent activation energy at the temperature T_{avg}, where

$$T_{avg} = \frac{2\,T_1T_2}{T_1 + T_2}$$

In the current investigation, $T_{avg} \approx 811$°K (1000°F). The calculated average value of Q_a was 94,650 cal/mole, which was considerably higher than the value reported by Ishida, et al. for creep in pure iron.[56] Ishida, et al. also indicated that the value they obtained for the activation energy for creep in pure iron was in close agreement with the activation energy for self-diffusion in pure iron, i.e. 68,000 cal/mole. Therefore, the apparent activation energy for creep in alloy Ta7Cr was higher than that for creep in pure iron, and for self-diffusion in pure iron. As stated earlier, values of apparent activation energy considerably higher than those for matrix self-diffusion have been observed in the creep of other dispersion strengthened materials.[31,44,47,48]

The structural changes during creep, and the observed activation energy and stress sensitivity of creep rate in alloy Ta7Cr appeared to indicate that there was no single rate-controlling step during creep at 1100°F (593°C). If dislocation climb was the only rate-controlling factor, then the apparent activation energy for creep would be expected to be equal to the activation energy for self-diffusion in the matrix.

As was stated earlier, the apparent activation energy for creep in alloy Ta7Cr was higher than the activation energy for self-diffusion. This indicated that creep models based on dislocation climb as the only rate controlling step[32-34,43-45] were not applicable to alloy Ta7Cr. The generation of dislocations at grain boundary dislocation sources in the manner suggested by Ansell and Weertman[44] was not required for creep deformation to occur in alloy Ta7Cr since there was a high density of mobile dislocations in the alloy before creep, as was shown in Figs. 12 and 13. Creep models based on cross slip of piled up dislocations[31,33] as the only rate-controlling process were not applicable to alloy Ta7Cr since the activation energy for cross slip-controlled creep generally never exceeds the activation energy for self-diffusion in the matrix.

The high values of measured apparent activation energy and stress sensitivity exponent in addition to the several substructural features suggested that creep in alloy Ta7Cr involved two or more processes acting in parallel. Multistep reactions in creep have been proposed by several other investigators.[57-60] Gilbert and Munson[60] suggested that creep can occur by two, and possibly more, steps acting in parallel. In their investigation, the steps were: (1) Initial glide of dislocations leading to pile-ups at barriers, and subsequent creep by a mechanism based on dislocation climb at thermal jogs, (2) Glide of dislocations resulting in dislocation intersection and jog formation, and subsequent climb of jogged dislocations; both jog formation and climb are aided by temperature and stress, and (3) Climb of dislocations by vacancy diffusion in the matrix. They concluded that these different steps could act independent of each other in parallel, and thus lead to apparent creep activation energies higher than the activation energy for matrix self-diffusion. The experimental results of the present investigation suggested that creep of alloy Ta7Cr possibly involved parallel and independent steps similar to those proposed by Gilbert and Munson.[60] In this alloy the Laves phase particles formed effective barriers to dislocation glide leading to dislocation pile-ups and substructure pinning as was discussed earlier. It was also probable that at 1200°F (649°C), grain boundary deformation contributed to creep deformation and constituted an additional step in parallel. Evidence of grain boundary deformation was presented in an earlier section. Observations indicating intergranular nucleation of voids leading to intergranular cracks are discussed in the section on creep fractures.

J. Effect of Alloying Additions of Molybdenum on the Creep Properties of Alloy Ta7Cr

The study of tensile and creep properties, and the examination of structural features of specimens of alloy Ta7Cr before and after creep testing indicated that partial recovery of dislocation substructure occurred in the alloy. This was particularly evident in specimens exposed for a long time (1809 hrs) at 1100°F (593°C) and for a relatively shorter time (119 hrs) at 1200°F (649°C). It was of interest to examine if further alloying by solid solution strengthening would enhance creep strength by retarding recovery. Molybdenum was chosen as the alloying element for this purpose, since it is well known[61-65] that molybdenum additions are very effective in attaining solid solution strengthening in elevated temperature alloys and the strengthening so attained is retained at elevated temperatures.

The addition of 0.5 atom pct Mo to alloy Ta7Cr, leading to the alloy Ta7CrMo, caused a considerable change in the kinetics of the α→γ transformation. The transformation exhibited a unique time-temperature dependence which is discussed in detail elsewhere.[25] At the spheroidizing temperature of 1100°C, a 10 min hold time was not sufficient for completion of the α→γ transformation. A treatment consisting of three repeated heating and cooling cycles between room temperature and 1100°C, however, resulted in completion of the transformation. During each cycle a specimen was held at 1100°C for 15 min. before it was air cooled to room temperature. The creep and stress rupture properties discussed in this section for alloy Ta7CrMo were for the spheroidizing treatment of three 15 min. cycles at 1100°C following one hour solution treating at 1350°C and one hour aging to attain peak hardness at 700°C.

In Fig. 39 is shown the plot of stress vs rupture time at 1100°F (593°C) for alloy Ta7CrMo. Also shown in the figure are the results for alloy Ta7Cr and the properties quoted in the literature[37] for several commercial steels. It was evident that the alloy Ta7CrMo had considerably higher rupture strength than alloy Ta7Cr. The rupture strength approached that of Greek Ascoloy.

The plot of applied stress vs. steady state creep rate of alloy Ta7CrMo is shown in Fig. 40 for a test temperature of 1100°F (593°C). Also shown is a similar plot for alloy Ta7Cr (Heat Treatment T-1). The higher creep strength (lower creep rates) of alloy Ta7CrMo compared to that of alloy Ta7Cr is clearly evident. The stress for a creep state of 1×10^{-4} pct/hr at 1100°F (593°C) for alloy Ta7CrMo was determined from Fig. 40, and was 15,000 psi. This value is compared in Table XIII with the values for alloy Ta7Cr and several commercial ferritic steels.[37,40] The comparison revealed that the creep strength of alloy Ta7CrMo was only slightly lower than that of type 422 stainless steel.

Additional improvements attained in the creep properties of alloy Ta7CrMo by modifications in the heat treating procedure are reported elsewhere.[25,29]

K. Mechanism of Fracture of Alloy Ta7Cr Tested in Creep

In Fig. 41 are shown scanning electron fractographs of specimens of alloy Ta7Cr (Heat Treatment T-1) tested at 1000°F (538°C) and a constant stress of 42,500 psi. The rupture time at this stress was 3.5 hrs. An examination of the fractograph shown in Fig. 41(a) revealed dimpled rupture typical of a ductile fracture mode. There were two ranges of dimple sizes, large and small. The large dimples were associated with voids around precipitate particles of diameter approximately 1 μ to 4 μ. The areas between large dimples consisted of small dimples, a number of which were associated with voids around small preciptate particles of less than 1 μ diameter. A small dimple formed around a small precipitate particle is indicated by an arrow in Fig. 41(b). Another feature that is observed in Fig. 41 is evidence of ductile tearing, which also resulted in a dimpled appearance (Fig. 41(a)). The observations suggested that fracture of the specimen tested at 1000°F (538°C) and 42,500 psi was initiated by failure of the precipitate-matrix interface. Interface failure resulted in the formation of voids. When voids occupied a large fraction of the specimen cross sectional area, the remaining area failed by ductile tearing.

As the stress was decreased at 1000°F (538°C), rupture time increased, and this resulted in changes in the overall fracture appearance. Scanning electron fractographs of specimens of alloy Ta7Cr tested at 1000°F (538°C) at several indicated constant stresses are shown in Fig. 42. The rupture times at the various stresses are also indicated in Fig. 42. It was noted that with increase in rupture time, the extent of ductile tearing decreased, and a larger portion of the fracture surface exhibited large dimples nucleated at precipitate particles. As shown in Fig. 42(d), the fracture surface of the specimen of alloy Ta7Cr tested at 1000°F (538°C) and 27,000 psi to give a rupture time of 1181 hrs consisted almost entirely of large (at A) and small (at B) dimples nucleated at precipitate particles. There was no evidence of intergranular failure in specimens of alloy Ta7Cr (Heat Treatment T-1) tested at 1000°F (538°C).

Scanning electron fractographs of specimens of alloy Ta7Cr (Heat Treatment T-1) tested at several constant stresses at 1100°F (593°C) revealed fracture features similar to those in specimens tested at 1000°F (538°C). In Fig. 43 are shown scanning electron fractographs of the alloy tested at 1100°F (593°C) and 15,000 psi. The rupture time for the specimen was 1809 hrs. Large dimples formed by void nucleation and growth around precipitate particles are clearly seen in Fig. 43(a). Small dimples, also formed by void nucleation and growth around precipitate particles are shown in Fig. 43(b) in the area around A. There is no evidence of intergranular failure in Fig. 43. However, an examination, by optical metallography, of longitudinal sections of the gage length of the creep specimen indicated that void nucleation and growth did occur at grain boundaries in some parts of the specimen. Examples of these voids are shown by arrows in Fig. 44(a) and (b). Apparently these voids did not play an important role in final fracture.

A large number of intergranular voids were noted in a specimen of alloy Ta7Cr (Heat Treatment T-1) tested to rupture at 1200°F (649°C) and 11,000 psi. The rupture time under these conditions was 119 hrs. Figure 45 shows an optical micrograph of a longitudinal section of the fractured specimen. Intergranular voids are indicated by arrows in Fig. 45. Scanning electron fractographs of the same specimen are shown in Fig. 46. Dimpled rupture caused by void nucleation and growth around precipitate particles was evident as in the case of specimens tested at 1000°F (538°C) and 1100°F (593°C). In addition, there was evidence of intergranular failure caused by crack initiation and growth at grain boundaries and triple points, as indicated by arrows in Fig. 46(b) and (c). Several investigators[66 70] have reported that at high temperatures, deformation at grain boundaries and triple points leads to void formation at second phase particles and ledges at these locations. Subsequent growth of these voids during creep leads to the formation of cracks. Final failure then occurs by transgranular crack propagation.

In summary, fracture of spheroidized alloy Ta7Cr in stress rupture tests at temperatures 1000-1200°F (538-649°C) occurred by formation and growth of voids around particles of the Laves phase. Larger particles appeared to play the major role in crack initiation. Voids formed intergranularly in long time tests at 1100°F (593°C), but did not cause intergranular fracture. On the other hand, extensive intergranular void formation at 1200°F (649°C) significantly contributed to crack initiation and final fracture.

V. SUMMARY AND CONCLUSIONS

The strengthening effect of the Laves phase in Fe-Ta alloys was utilized to develop creep resistant body centered cubic iron alloys containing 1 at.pct. Ta and up to 7 at.pct. Cr. Precipitation of the Fe-Ta Laves phase led to considerable hardening of Fe-Ta-Cr alloys, but precipitation occurred heterogeneously at grain boundaries and other preferred sites, leading to room temperature embrittlement. The embrittlement was overcome by using an allotropic phase transformation to spheroidize the Laves phase precipitate at the grain boundaries and within the grains. The structure of a spheroidized alloy Ta7Cr, containing 1 at.pct. Ta and 7 at.pct. Cr, was characterized by a uniform distribution of almost spherical particles of the Fe-Ta Laves phase in a body centered cubic matrix with irregular grain boundaries. Particle diameters of the precipitate ranged from 0.03 to 4 μ. Examination by transmission electron microscopy revealed a lath-like substructure with irregular subgrains and tangled dislocation networks in the laths. The dislocation substructure was pinned in a few instances by the precipitate particles, but a high density of unpinned dislocations was present.

Both the aged, and aged and spheroidized Fe-Ta-Cr alloys maintained considerable fractions of their room temperature yield and ultimate strengths up to a test temperature of about 600°C. At temperatures higher than about 600°C, the yield and ultimate tensile strengths decreased sharply. Variations in the heat treating procedure, involving cold working before aging, and repeated cycling between room temperature and the spheroidizing temperature, did not cause significant changes in short-time tensile properties of alloy Ta7Cr, particularly at test temperatures in the neighborhood of 700°C. A substructure developed by cold working the spheroidized Ta7Cr alloy was not effectively retained by the alloy at temperatures higher than about 700°C.

Constant load creep and stress rupture tests were conducted on spheroidized alloy Ta7Cr at several stresses and temperatures. The results indicated that, in general, the rupture strength of alloy Ta7Cr was higher than that of ferritic steels containing 5 to 12 pct. Cr and strengthened by dispersions of chromium and molybdenum carbides, but lower than that of ferritic steels containing significant amounts of vanadium and tungsten as solid solution strengtheners and carbide formers. The steel 0.3C-1Cr-1Mo-0.25V had a higher rupture strength, but lower creep strength than alloy Ta7Cr at 1000°F (538°C).

Transmission electron microscopic examinations of the substructure of crept specimens of alloy Ta7Cr revealed dislocation pile-ups, jogs, and a well developed subgrain structure with low dislocation density within the subgrains. In long time exposures at 1100°F (593°C) and 1200°F (649°C) precipitation of the Laves phase occurred during creep. The particles that were observed in a specimen tested in creep at 1100°F (593°C) were of diameters less than about 0.03 μ. Both the coarser precipitate particles originally present, and the finer particles precipitated during creep were found to act as pinning points for individual dislocations and subgrain boundaries and possibly played an important role in retarding the complete recovery of dislocation substructure. Specimens tested in creep at 1200°F (649°C) showed evidence of grain boundary deformation.

The measured apparent activation energy for creep of alloy Ta7Cr was higher than the activation energy for self diffusion in iron, and the estimated value of the stress sensitivity exponent was higher than the value observed for iron. These observations, and a study of the structural changes during creep suggested that the creep of alloy Ta7Cr involved two or more independent rate-controlling processes in parallel.

Solid solution alloying additions of small amounts of molybdenum considerably improved the rupture strength and creep resistance of alloy Ta7Cr.

Examination of the fracture surfaces of specimens tested to rupture at several constant loads and temperatures indicated that fracture occurred by nucleation and growth of voids around particles of the Laves phase precipitate, leading to ductile failure characterized by a dimpled fracture appearance. Particles of diameters 1 μ to 4 μ appeared to play a more predominant role in fracture initiation than finer particles.

Examintaion, by optical microscopy, of longitudinal sections of a creep specimen tested to rupture in 1809 hrs at 1100°F (593°C) and 15,000 psi revealed intergranular cracks, but these cracks did not propagate to cause intergranular fracture. A combination of optical and scanning electron microscopy showed that intergranular void nucleation and crack formation were extensive in specimens tested under creep conditions at 1200°F (649°C), and final fracture resulted due to the propagation of several intergranular cracks.

ACKNOWLEDGEMENTS

The author wishes to express his deep appreciation to Professor Victor F. Zackay and Professor Earl R. Parker for their constant encouragement and guidance during the course of this investigation. He would also like to express his gratitude to Professor Iain Finnie for a critical review of the manuscript. Special thanks are extended to Mr. M. S. Bhat and Dr. Michael Yokota for many discussions and help in electron microscopy.

The valuable assistance provided by the technical support staff of the Inorganic Materials REsearch Division is acknowledged; thanks are due, in particular, to John Holthuis (alloy Processing), Don Krieger (elevated temperature tensile testing), Lee Johnson (metallography and zone refining), Julien Patenaude (machining), Gloria Pelatowski (preparation of line drawings), Doug Kreitz and Phila Witherell (technical photography), and Alice Ramirez, Jean Wolslegel and Shirley Ashley (manuscript preparation). Appreciation is also extended to Anamet Laboratories, Berkeley for making available the equipment for creep and stress rupture testing.

This work was done under the auspices of the United States Atomic Energy Commission.

REFERENCES

1. R. W. Guard, Mechanical Behavior of Materials at Elevated Temperatures, J. E. Dorn, ed. (McGraw-Hill Book Co., Inc., New York, 1961), p. 270.
2. L. H. Toft and R. A. Marsden, Iron Steel Inst. Spec. Rep. No. 70, p. 276, 1961.
3. E. W. Colbeck and J. R. Rait, Symp. High Temperature Steels and Alloys for Gas Turbines, Iron Steel Inst. Rep. No. 43, p. 107, 1952.
4. G. A. Mellor and S. M. Barker, J. Iron Steel Inst. 194, 464 (1960).
5. J. H. Woodhead and A. G. Quarrell, J. Iron Steel Inst. 203, 605 (1965).
6. R. F. Decker and S. Floreen, Precipitation from Iron-Base Alloys, G. R. Spiech and J. B. Clark, eds., AIME Met. Soc. Conf. Vol. 28 (Gordon and Breach Science Publishers, New York, 1965), p. 69.
7. R. F. Decker, Steel Strengthening Mechanisms, Symp. sponsored by Climax Molybdenum Co., 1969, p. 147.
8. J. R. Mihalisin, C. C. Bieber and R. T. Grant, Trans. Met. Soc. AIME 242, 2399 (1968).
9. M. G. Gemmill, H. Hughes, J. D. Murray, F. B. Pickering and K. W. Andrews, J. Iron Steel Inst. 184, 122 (1956).
10. V. F. Zackay, E. R. Parker and D. Bhandarkar, Proc. John E. Dorn Memorial Symp. on Rate Processes in Plastic Deformation, Cleveland, Ohio, October 1972. Also LBL-1174, Lawrence Berkeley Laboratory, Berkeley, California, October 1972.

11. R. H. Jones, E. R. Parker and V. F. Zackay, Proc. Fifth Intern. Mater. Symp., Berkeley, California, September 1971, p. 829.

12. S. Jin, M.S. thesis, LBL Rep. 443, University of California, Berkeley, California, December 1971.

13. A. K. Sinha and W. Hume-Rothery, J. Iron Steel Inst., 205, p. 671 (1967).

14. H. J. Wallbaum, Z. Krist., 103, p. 391 (1941).

15. M. Hansen, Constitution of Binary Alloys, 2nd Edition, (McGraw-Hill Book Co., Inc., New York, 1958), p. 720.

16. R. P. Elliott, Constitution of Binary Alloys, First Supplement, (McGraw-Hill Book Co., Inc., New York, 1965), p. 255.

17. L. Brewer, High Strength Materials, V. F. Zackay, ed., (John Wiley and Sons, Inc., New York, 1965), p. 12.

18. R. H. Jones, Ph. D. Thesis, LBL Rep. 179, University of California, Berkeley, California, October 1971.

19. R. H. Jones, V. F. Zackay and E. R. Parker, Met. Trans., 3, p. 2835 (1972).

20. G. R. Speich and H. Warlimont, J. Iron Steel Inst., 206, p. 385 (1968).

21. J. B. Massalski, Phase Transformations, (American Soc. for Metals, Metals Park, Ohio, 1970), p. 433.

22. A. Baghdasarian, To be published.

23. M. Hansen, Constitution of Binary Alloys, 2nd Edition, (McGraw-Hill Book Co., Inc., New York, 1958), p. 525.

24. Welding Handbook, Section 4, A. L. Phillips ed., 5th edition, (American Welding Society, New York, New York, 1966), p. 643.

25. M. S. Bhat, M.S. Thesis, University of California, Berkeley, California (to be published).

26. V. K. Lindroos and K. O. Vilpponen, Proc. Fifth Intern. Mater. Symp., Berkeley, California, September 1971, p. 732.

27. A. S. Keh, W. C. Leslie and G. R. Speich, Symp. on the Role of Substructure in Mechanical Behavior of Metals, Tech. Documentary Rep. No. ASD-TDR-63-324, p. 393, Wright Patterson Air Force Base, Ohio, April 1963.

28. J. D. Cook and J. Nutting, *The Mechanism of Phase Transformations in Crystalline Solids*, (Institute of Metals, London 1969), p. 54.

29. D. Bhandarkar, M. S. Bhat, V. F. Zackay and E. R. Parker (in preparation).

30. C. L. Meyers and O. D. Sherby, J. Inst. Metals, 90, p. 380 (1962).

31. B. A. Wilcox and A. H. Clauer, Trans. Met. Soc. AIME, 236, p. 570 (1966).

32. A. H. Clauer and B. A. Wilcox, Met. Sci. J., 1, p. 86 (1967).

33. B. A. Wilcox and A. H. Clauer, *Oxide Dispersion Strengthening*, G. S. Ansell, T. D. Cooper and F. V. Lenel eds., AIME Met. Soc. Conf., Vol. 47, (Gordon and Breach Science Publishers, New York, 1968), p. 323.

34. B. A. Wilcox and A. H. Clauer, Met. Sci. J., 3, p. 26 (1969).

35. G. J. P. Buchi, J. H. R. Page, and M. P. Sidey, J. Iron Steel Inst., 203, p. 291 (1965).

36. R. Pilkington, G. Willoughby and J. Barford, Met. Sci. J., 5, p. 1, (1971).

37. Metals Handbook, Vol. 1, (American Society for Metals, Metals Park, Ohio, 1968).

38. D. A. Oliver and G. T. Harris, Metallurgia, 34, p. 293 (1946).

39. K. E. Amin and J. E. Dorn, Acta Met., 17, p. 1429 (1969).

40. F. J. Clauss, Engineers Guide to High Temperature Materials, (Addison and Wesley Publishing Co., Inc., Reading, Massachusetts, 1971).

41. W. Betteridge and J. A. Towers, J. Iron Steel Inst., 191, p. 235 (1959).

42. E. R. Parker, Private communication.

43. J. Weertman, J. App. Phy., 28, p. 362 (1957).

44. G. S. Ansell and J. Weertman, Trans. Met. Soc. AIME 215, p. 838 (1959).

45. G. S. Ansell and F. V. Lenel, Trans. Met. Soc. AIME, 221, p. 452 (1961).

46. D. Sidey and B. Wilshire, Met. Sci. J., 3, p. 56 (1969).

47. K. Milicka, J. Cadek and P. Rys, Acta Met., 18, p. 733 (1970).

48. A. Lasalmonie and M. Sindzingre, Acta Met., 19, p. 57 (1971).

49. S. Takahashi, K. Iida and M. Adachi, Trans. Nat. Res. Inst. Metals, Tokyo, 6, p. 231 (1964).

50. S. Takahashi, K. Iida and M. Adachi, ibid, p. 376.

51. R. Lagneborg, Met. Sci. J., 3, p. 18 (1969).

52. J. J. Petrovic and L. J. Ebert, Met. Trans., 4, p. 1309 (1973).

53. F. V. Nolfi, Jr., and C. A. Johnson, Acta Met., 20, p. 769 (1972).

54. R. Lagneborg, Intern. Met. Rev., 17, p. 130 (1972).

55. T. E. Tietz and J. E. Dorn, Trans Met. Soc. AIME 206, p. 156 (1956).

56. Y. Ishida, C. Cheng and J. E. Dorn, Trans. Met. Soc. AIME, 236, p. 964 (1966).

57. O. D. Sherby, J. L. Lytton and J. E. Dorn, Acta Met., 5, p. 219 (1957).

58. W. J. M. Tegart and O. D. Sherby, Phil. Mag., 3, p. 1287 (1958).

59. C. Crussard and R. Tamhanker, Trans. Met. Soc. AIME, 212, p. 718 (1958).

60. E. R. Gilbert and D. E. Munson, Trans. Met. Soc. AIME, 233, p. 429 (1965).

61. C. R. Austin, C. R. St. John and R. W. Lindsay, Trans. Met. Soc. AIME, 162, p. 84 (1945).

62. S. F. Reiter and W. R. Hibbard, Jr., Trans. Met. Soc. AIME, 203, p. 655 (1955).

63. E. R. Parker, Proc. ASTM, 60, p. 1 (1960).

64. G. A. Mellor and S. M. Barker, J. Iron Steel Inst., 194, p. 464 (1960).

65. B. B. Argent, M. N. van Niekerk and G. A. Redfern, J. Iron Steel Inst., 208, p. 830 (1970).

66. J. E. Harris, Trans. Met. Soc. AIME, 233, p. 1509 (1965).

67. L. J. Barker and D. M. R. Taplin, Acta Met., 14, p. 1527 (1966).

68. E. Smith and J. T. Barnby, Met. Sci. J., 1, p. 1 (1967).

69. P. W. Davies and K. R. Williams, Met. Sci. J., 3, p. 48 (1969).

70. H. R. Tipler, L. H. Taylor, and B. E. Hopkins, Met. Sci. J., 4, p. 167 (1970).

Table I. Chemical Compositions of Alloys

Alloy Designation	Compositions							
	Wt. Pct.				At. Pct.			
	Ta	Cr	Mo	Fe	Ta	Cr	Mo	Fe
Ta5Cr	3.18	4.57	--	Bal	1	5	-	Bal
Ta7Cr	3.18	6.40	--	Bal	1	7	-	Bal
Ta7CrMo	3.17	6.38	0.84	Bal	1	7	0.5	Bal

Table II. Heat Treatments and Designations

Heat Treatment	Designation
Solution treated at 1320°C for 1 hour, and aged at 700°C for 40 minutes.	T-0
Solution treated at 1320°C for 1 hour, aged at 700°C for 40 minutes, and spheroidized at 1100°C for 10 minutes.	T-1
Solution treated at 1320°C for 1 hour, aged at 700°C for 40 minutes, and cycled 3 times between 1100°C and 22°C. Holding time at 1100°C was 10 minutes each time.	T-2
Solution treated at 1320°C for 1 hour, cold rolled to a 50 pct. reduction in thickness at 22°C, aged at 700°C for 40 minutes, and spheroidized at 1100°C for 10 minutes.	T-3
Solution treated at 1320°C for 1 hour, aged at 700°C for 2 hours, and spheroidized at 1100°C for 10 minutes	T-4
Heat treated as for T-1, and cold rolled at 22°C to a 20 pct. reduction in thickness.	T-5

Table III. Short-time tensile mechanical properties of alloy Ta7Cr aged for 40 minutes at 700°C (Heat Treatment T-0).

Test Temp., °C	Yield Strength, Psi	Ultimate Tensile Strength, Psi	Fracture Elongation, Pct.
22	43,500	79,100	13.2
200	38,700	64,600	15.1
400	35,200	54,700	17.8
600	30,300	37,700	22.4
700	21,800	24,300	27.1

Table IV. Short-time tensile mechanical properties of alloy Ta7Cr spheroidized for 10 minutes at 1100°C (Heat Treatment T-1).

Test Temp., °C	Yield Strength, Psi	Ultimate Tensile Strength, Psi	Fracture Elongation, Pct.
22	61,300	81,700	20.7
200	55,900	67,800	17.8
400	54,900	62,500	14.0
600	44,200	46,400	18.4
700	20,500	21,900	24.4

Table V. Short-time tensile yield strength of Fe-Ta-Cr alloys at room and elevated temperatures.

Alloy	Heat Treatment	Test Temperature (°C) and 0.2 Pct. Offset Yield Strength (psi)				
		22	200	400	600	700
Ta5Cr	T-1	44,800	35,700	34,000	27,600	19,000
Ta7Cr	T-0	43,500	38,700	35,200	30,300	21,800
Ta7Cr	T-1	61,300	55,900	54,900	44,200	20,500
Ta7Cr	T-2	64,000	58,100	53,200	38,800	23,500
Ta7Cr	T-3	58,100	-	47,200	41,500	23,200
Ta7Cr	T-4	63,900	-	-	41,500	-
Fe-1Ta*	T-1	38,000	34,500	30,000	26,000	16,000

*Data from Jones, et al.[21] The heat treatment was T-1 except that the solution treating temperature was 1400°C and the aging time was 1 hour.

Table VI. Short-time ultimate tensile strength of Fe-Ta-Cr alloys at room and elevated temperatures.

Alloy	Heat Treatment	Test Temperature (°C) and Ultimate Tensile Strength (psi)				
		22	200	400	600	700
Ta5Cr	T-1	74,500	56,600	49,000	34,700	19,800
Ta7Cr	T-0	79,100	64,600	54,700	37,700	24,300
Ta7Cr	T-1	81,700	67,800	62,500	46,400	21,900
Ta7Cr	T-2	82,900	68,300	60,300	43,000	24,200
Ta7Cr	T-3	84,200	-	59,500	43,700	23,900
Ta7Cr	T-4	81,200	-	-	43,500	-

Table VII. Fracture elongation of Fe-Ta-Cr alloys in short-time tensile tests at room and elevated temperatures.

Alloy	Heat Treatment	Test Temperature (°C) and Fracture Elongation (pct)				
		22	200	400	600	700
Ta5Cr	T-1	24.8	20.0	18.2	29.8	32.3
Ta7Cr	T-0	13.2	15.1	17.8	22.4	27.1
Ta7Cr	T-1	20.7	17.8	14.0	18.4	24.4
Ta7Cr	T-2	24.2	18.1	14.7	21.3	34.7
Ta7Cr	T-3	15.2	-	18.1	20.5	26.3
Ta7Cr	T-4	18.8	-	-	16.3	-

Table VIII. Short-time tensile mechanical properties of alloy Ta7Cr in the spheroidized (Treatment T-1) and spheroidized and cold rolled (Treatment T-5) conditions.

Test Temp., °C	Yield Strength, Psi		Ultimate Tensile Strength, Psi		Fracture Elongation, Pct.	
	Treatment T-1	Treatment T-5	Treatment T-1	Treatment T-5	Treatment T-1	Treatment T-5
22	61,300	86,800	81,700	88,500	20.7	11.2
200	55,900	81,600	67,800	81,900	17.8	11.1
400	54,900	75,100	62,500	76,100	14.0	11.1
600	44,200	50,800	46,400	51,200	18.4	11.4
700	20,500	23,700	21,900	26,300	24.4	12.6

Table IX. Stress rupture properties of alloy Ta7Cr spheroidized at 1100°C for 10 minutes (Heat Treatment T-1).

Test Temp., °F	Stress, Psi	Rupture Time, Hrs.
900(482°C)	40,000	Did not rupture in 1272 Hrs.
1000(538°C)	27,000	1,181
	35,000	385
	38,000	185
	40,000	140
	42,500	3.5
1100(593°C)	10,000	Did not rupture in 1200 Hrs.
	15,000	1,809
	20,000	142
	25,000	27
	29,000	14
	30,500	1.3
1200(649°C)	11,000	119

Table X. The 1000 hour rupture stress at 1100°F(593°C) for alloy Ta7Cr and commercial steels.

Alloy	1000 Hour Rupture Stress, Psi
Ta7Cr	16,000
0.3C-1Cr-1Mo-0.25V Steel	36,900
0.15C-9Cr-1Mo Steel	14,100
0.15C-7Cr-0.5Mo Steel	13,300
403 and 410 Stainless	14,300
Greek Ascoloy	27,500
422 Stainless	33,800

Table XI. Steady state creep rates of alloy Ta7Cr spheroidized at 1100°C for 10 minutes (Heat Treatment T-1).

Test Temp., °F	Stress, Psi	Steady State Creep Rate, 10^{-4} Pct/Hr
900(482°C)	40,000	No steady state reached. After 1272 hrs. at stress, the creep rate still decreasing.
1000(538°C)	40,000	28.80
	38,000	13.72
	35,000	(a) 11.80
		(b) 15.00
	30,500	8.45
	27,000	(a) 2.84
		(b) 4.20
1100(593°C)	20,000	129.80
	15,000	21.20
	10,000	1.44
1200(649°C)	11,000	791

Table XII. Stress for a creep rate of 1×10^{-4} pct/hr at 1000°F (538°C) for alloy Ta7Cr and and commercial steels.

Alloy	Stress for Creep Rate of 1×10^{-4} Pct/Hr.
Ta7Cr	22,400
0.3C-1Cr-1Mo-0.25V Steel	16,700
0.15C-9Cr-1Mo Steel	12,500
0.15C-7Cr-0.5Mo Steel	8,800
403 and 410 Stainless	10,000
Greek Ascoloy	---
422 Stainless	39,000

Table XIII. Stress for a creep rate of 1×10^{-4} pct/hr at 1100°F(593°C) for alloy Ta7Cr, Ta7CrMo and commercial steels.

Alloy	Stress for Creep Rate of 1×10^{-4} Pct/Hr.
Ta7Cr	9,400
Ta7CrMo	15,000
0.3C-1Cr-1Mo-0.25 Steel	---
0.15C-9Cr-1Mo Steel	6,300
0.15C-7Cr-0.5Mo Steel	4,000
403 and 410 Stainless	4,000
Greek Ascoloy	---*
422 Stainless	19,000

*Creep strength very low and not quoted as it changes with time during the test.

FIGURE CAPTIONS

Fig. 1 A typical heat treating cycle for the Fe-Ta-Cr and Fe-Ta-Cr-Mo alloys of the present investigation.

Fig. 2 Schematic sketch of a sheet tensile specimen used for short-time tests at room and elevated temperatures.

Fig. 3 Sketch of a creep specimen used in the present investigation.

Fig. 4 Schematic diagram of the specimen and extensometer assembly for creep and stress rupture tests.

Fig. 5 Iron-rich portion of the equilibrium phase diagram of the Fe-Ta system.

Fig. 6 The variations of the room temperature microhardness of alloy Ta7Cr with aging time at 700°C. The alloy was solution treated at 1320°C for one hour and hot water quenched prior to aging.

Fig. 7 Optical micrograph showing the microstructure alloy Ta7Cr solution treated at 1320°C for one hour and aged at 700°C for 40 minutes.

Fig. 8 Transmission electron micrograph of a carbon replica showing the Laves phase particles extracted from alloy Ta7Cr. The alloy was solution treated at 1320°C for one hour, quenched, and aged at 700°C for 40 minutes prior to extraction of precipitate.

Fig. 9 Optical micrograph showing the microstructure of alloy Ta7Cr spheroidized at 1100°C for 10 minutes. (Heat Treatment T-1.)

Fig. 10 Transmission electron micrograph of a carbon replica showing the Laves phase particles extracted from alloy Ta7Cr spheroidized at 1100°C for 10 minutes. (Heat Treatment T-1.)

Fig. 11. Transmission electron micrograph of a thin foil specimen of alloy Ta7Cr (Heat Treatment T-1) showing a uniform distribution of almost spherical particles of the Laves phase in a matrix characterized by a lath-like substructure.

Fig. 12. Transmission electron micrographs of a thin foil specimen of alloy Ta7Cr (Heat Treatment T-1) under two-beam diffracting conditions with operating g-vectors of $[01\bar{1}]$ in (a) and $[0\bar{3}1]$ in (b).

Fig. 13. Transmission electron micrographs of a thin foil specimen of alloy Ta7Cr (Heat Treatment T-1):

(a) Bright field showing the dislocation substructure

(b) Selected area diffraction pattern obtained from the area enclosed by the image of the aperture in (a). Matrix reflections of {110} type are marked 1,2,4 and 5.

Fig. 14. Effect of test temperature on the short-time yield strength, ultimate tensile strength, and fracture elongation of alloy Ta7Cr (Heat Treatment T-0).

Fig. 15. Scanning electron fractographs of alloy Ta7Cr (Heat Treatment T-0) tested in short-time tensile tests at (a) 22°C; (b) 200°C; (c) 400°C, and (d) 600°C.

Fig. 16. Scanning electron fractographs of alloy Ta7Cr tested in short-time tensile tests at 22°C following (a) Heat Treatment T-1 and (b) Heat Treatment T-0.

Fig. 17. Effect of test temperature on the short-time yield strength, ultimate tensile strength, and fracture elongation of alloy Ta7Cr (Heat Treatment T-1).

Fig. 18. Yield strength vs. test temperature for alloy Ta7Cr heat treated by processes T-1, T-2, T-3 and T-4.

Fig. 19. Yield strength vs. test temperature for spheroidized (Heat Treatment T-1), and spheroidized and cold worked (Heat Treatment T-5) alloy Ta7Cr.

Fig. 20. Stress vs. rupture time at test temperatures 1000°F (538°C) and 1100°F (593°C) for alloy Ta7Cr (Heat Treatment T-1).

Fig. 21. Stress vs. rupture time at 1000°F (538°C) for alloy Ta7Cr (Heat Treatment T-1). Also shown are the results reported in the literature (37) for 0.3C-1Cr-1Mo-0.25V steel, 0.15C-9Cr-1Mo steel, AISI types 403, 410 and 422 stainless steels, and Greek Ascoloy.

Fig. 22. Stress vs. rupture time at 1100°F (593°C) for the alloys mentioned in Fig. 21.

Fig. 23. Stress vs. steady state creep rate of alloy Ta7Cr (Heat Treatment T-1), at test temperatures indicated.

Fig. 24. Transmission electron micrograph of a thin foil specimen of alloy Ta7Cr (Heat Treatment T-1) tested in creep at 1100°F (593°C) and 15,000 psi, showing the precipitate distribution.

Fig. 25. Transmission electron micrographs of a thin foil specimen of alloy Ta7Cr (Heat Treatment T-1), tested in creep at 1100°F (593°C) and 15,000 psi:

(a) Bright field image.

(b) Selected area diffraction pattern obtained from the area enclosed by the image of the aperture in (a). Reflections A, B and C are from the Laves phase precipitate. Matrix reflection $(110)_M$ is marked.

(c) Dark field image of the reflection B showing reversal of contrast at precipitate particles.

Fig. 26. Plot of strain vs. time at 1100°F (593°C) and 15,000 psi for alloy Ta7Cr (Heat Treatment T-1).

Fig. 27. Transmission electron micrographs of thin foil specimens of alloy Ta7Cr (Heat Treatment T-1), tested in creep at 1100°F (593°C) and 15,000 psi. A well developed subgrain structure was observed with low dislocation density in the grain interiors. Pinning of subgrain boundaries and dislocations by precipitate particles was evident.

Fig. 28. Bright field transmission electron micrograph of a thin foil specimen of alloy Ta7Cr (Heat Treatment T-1), tested in creep at 1100°F (593°C) and 15,000 psi. The g-vector for the two-beam condition was $[2\bar{1}\bar{1}]$ as indicated. Dislocation pinning by both small and large Laves phase particles was noted.

Fig. 29. Bright field image of the area in Fig. 28 for a two-beam condition with $\bar{g} = [112]$ as indicated.

Fig. 30. Transmission electron micrograph of a thin foil specimen of alloy Ta7Cr (Heat Treatment T-1), tested in creep at 1100°F (593°C) and 15,000 psi, showing dislocations pinned by fine and coarse precipitate particles.

Fig. 31. Transmission electron micrograph of a thin foil specimen of alloy Ta7Cr (Heat Treatment T-1), tested in creep at 1100°F (593°C) and 15,000 psi, showing a dislocation pile-up at A.

Fig. 32 Transmission electron micrograph of a thin foil specimen of alloy Ta7Cr (Heat Treatment T-1), tested in creep at 1100°F (593°C) and 15,000 psi, showing dislocation jogs at A, B and C.

Fig. 33 Transmission electron micrograph of a thin foil specimen of alloy Ta7Cr (Heat Treatment T-1), tested in creep at 1200°F (649°C) and 11,000 psi:

(a) Bright field image for a two-beam case with $\bar{g} = [211]$.

(b) Selected area diffraction pattern obtained from the area enclosed by the image of the aperture in (a). Matrix reflection $(211)_M$ is marked.

Fig. 34 Transmission electron micrograph of a thin foil specimen of alloy Ta7Cr (Heat Treatment T-1), tested in creep at 1200°F (649°C) and 11,000 psi, showing dislocation pile-ups at A, B and C.

Fig. 35 Transmission electron micrograph of a thin foil specimen of alloy Ta7Cr (Heat Treatment T-1), tested in creep at 1200°F (649°C) and 11,000 psi, showing pinning of dislocations by precipitate particles near A.

Fig. 36 Transmission electron micrograph of a thin foil specimen of alloy Ta7Cr (Heat Treatment T-1), tested in creep at 1200°F (649°C) and 11,000 psi, showing pinning of subgrain boundaries by precipitate particles.

Fig. 37 Transmission electron micrograph of a thin foil specimen of alloy Ta7Cr (Heat Treatment T-1), tested in creep at 1200°F (649°C) and 11,000 psi, showing evidence of deformation at boundaries pinned by precipitate particles (at A, B and C).

Fig. 38 Transmission electron micrographs of thin foil specimens of alloy Ta7Cr:

- (a) After heat treatment T-1
- (b) After testing to rupture at 1100°F(593°C) and 15,000 psi
- (c) After testing to rupture at 1200°F(649°C) and 11,000 psi

Fig. 39 Stress vs. rupture time at 1100°F (593°C) for alloy Ta7CrMo, spheroidized by 3 cycles of $\alpha \rightarrow \gamma \rightarrow \alpha$ transformation following solution treating and aging. Also shown are the experimental results for alloy Ta7Cr, and the results reported in the literature (37) for 0.3C-1Cr-1Mo-0.25V steel, 0.15C-9Cr-1Mo steel, AISI types 403, 410, and 422 stainless steels and Greek Ascoloy.

Fig. 40 Stress vs. steady state creep rate at 1100°F (593°C) for alloy Ta7CrMo, spheroidized by 3 cycles of $\alpha \rightarrow \gamma \rightarrow \alpha$ transformation following solution treating and aging. Also shown are the experimental results on alloy Ta7Cr.

Fig. 41 Scanning electron fractographs of a specimen of alloy Ta7Cr (Heat Treatment T-1) tested to rupture at 1000°F (538°C) and 42,500 psi.

Fig. 42 Scanning electron fractographs of specimens of alloy Ta7Cr (Heat Treatment T-1) tested to rupture at 1000°F (538°C) and several indicated stresses:

- (a) 42,500 psi (rupture time = 3.5 hrs)
- (b) 40,000 psi (rupture time = 140 hrs)
- (c) 38,000 psi (rupture time = 185 hrs)
- (d) 27,000 psi (rupture time = 1181 hrs)

Fig. 43. Scanning electron fractographs of a specimen of alloy Ta7Cr (Heat Treatment T-1) tested to rupture at 1100°F (593°C) and 15,000 psi. Rupture time = 1809 hrs.

Fig. 44. Optical micrographs of a longitudinal section of a specimen of alloy Ta7Cr (Heat Treatment T-1) tested to rupture at 1100°F (593°C) and 15,000 psi. Intergranular voids are indicated by arrows.

Fig. 45. Optical micrograph of a longitudinal section of a specimen of alloy Ta7Cr (Heat Treatment T-1) tested to rupture at 1200°F (649°C) and 11,000 psi. Intergranular voids are indicated by arrows.

Fig. 46. Scanning electron fractographs of a specimen of alloy Ta7Cr (Heat Treatment T-1) tested to rupture at 1200°F (649°C) and 11,000 psi. The rupture time was 119 hrs. Arrows indicate cracks at grain triple points.

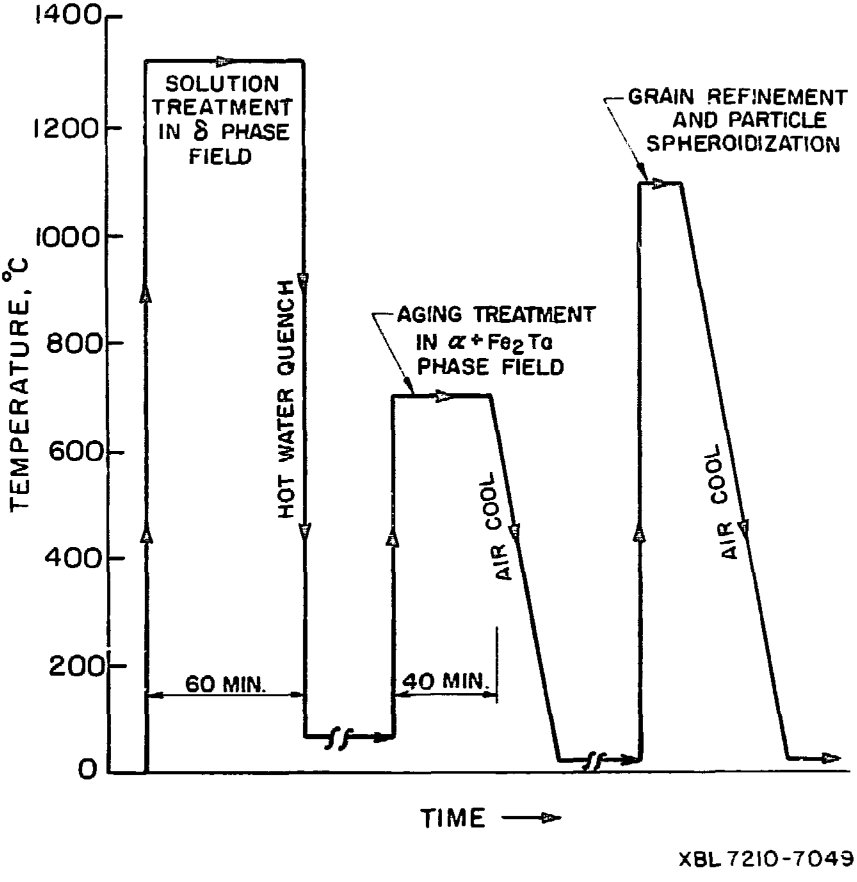
1400
1200
1000
800
600
400
200
0
TEMPERATURE, °C
TIME
SOLUTION TREATMENT IN δ PHASE FIELD
HOT WATER QUENCH
AGING TREATMENT IN α + Fe₂Ta PHASE FIELD
AIR COOL
GRAIN REFINEMENT AND PARTICLE SPHEROIDIZATION
AIR COOL
60 MIN.
40 MIN.
XBL 7210-7049

Fig. 1.

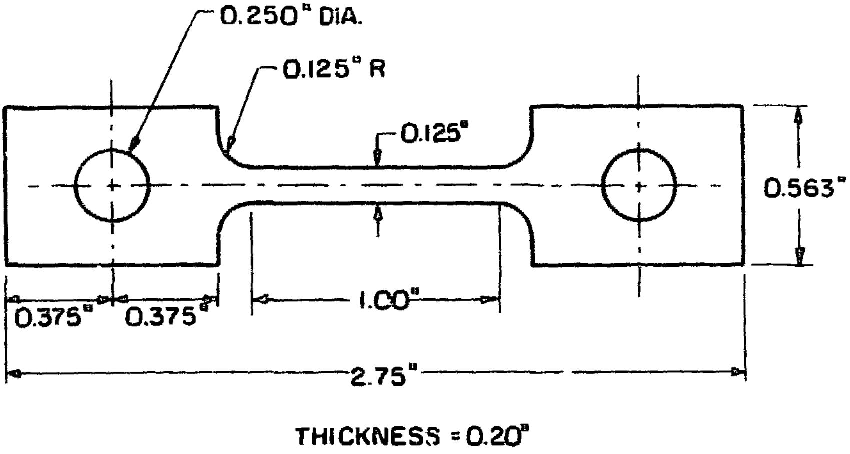

XBL737-6444

Fig. 2.

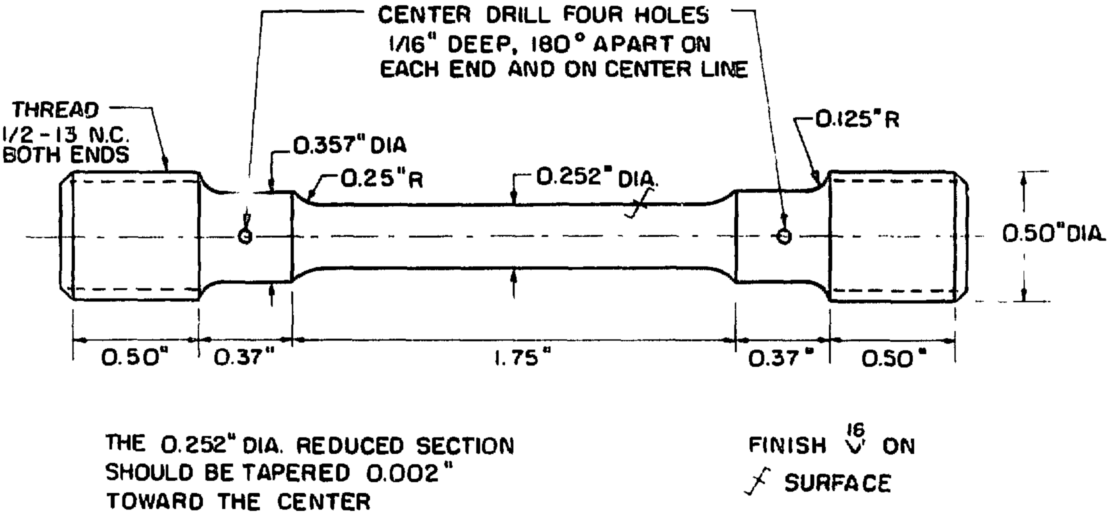

XBL737-6445

Fig. 3.

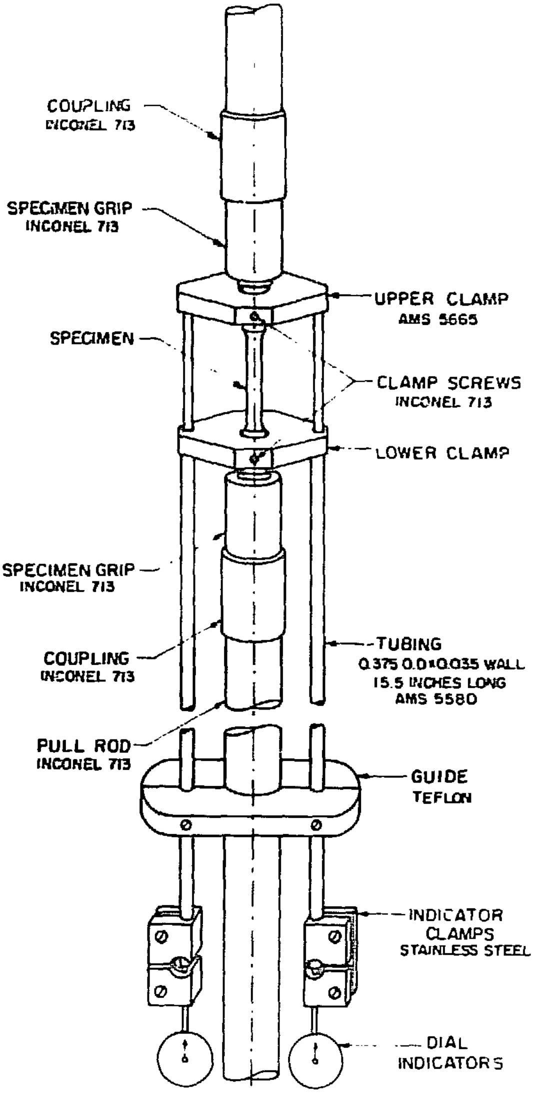

XBL 737-6446

Fig. 4.
]

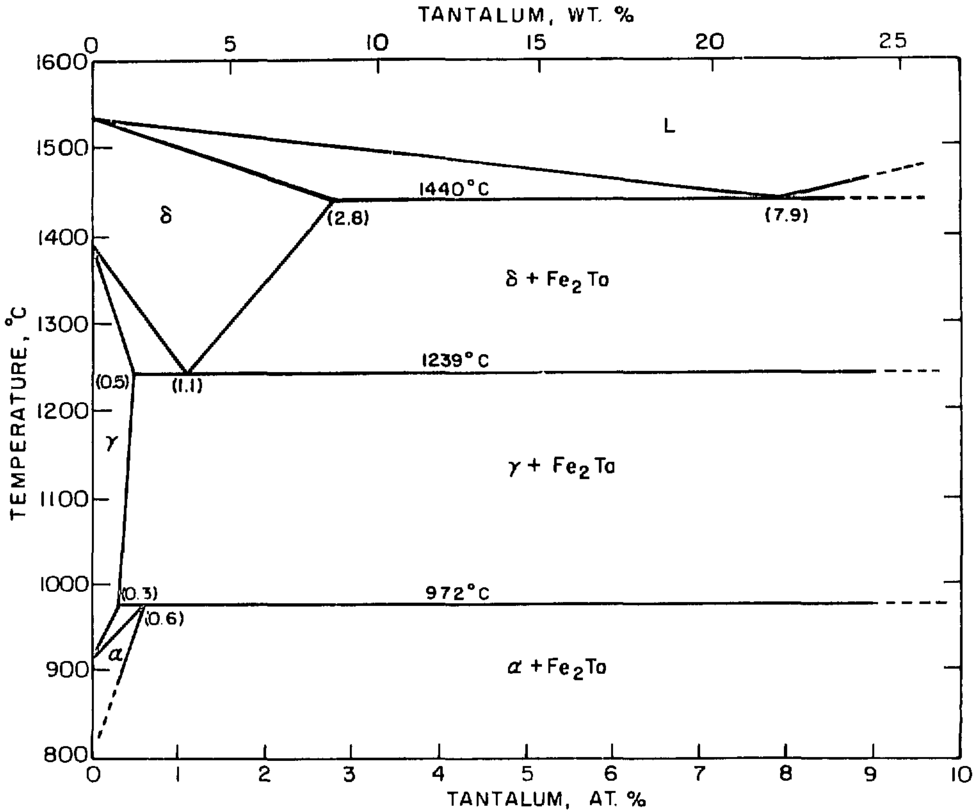

XBL721-5996

Fig. 5.

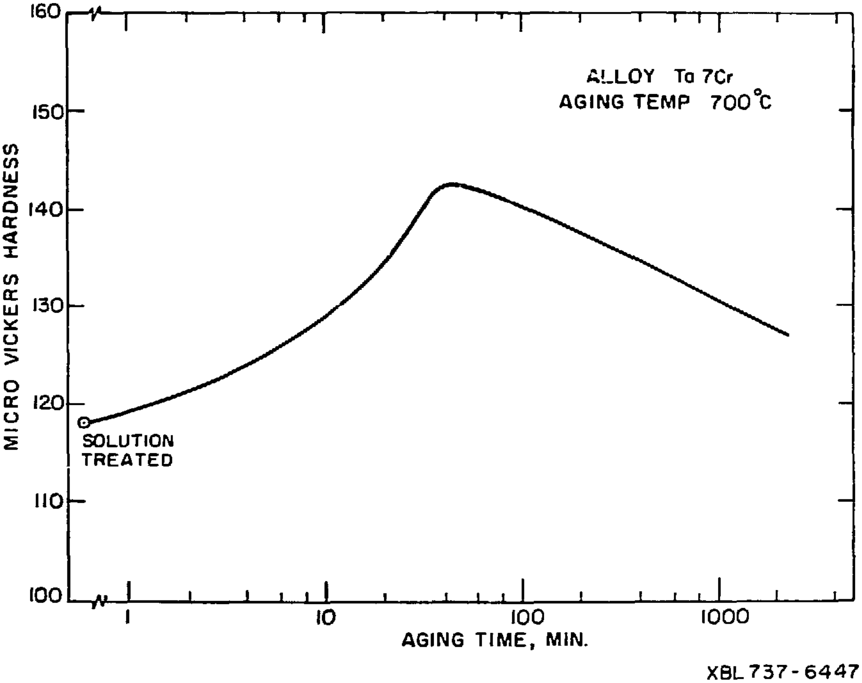
160
150
140
130
120
110
100
MICRO VICKERS HARDNESS
ALLOY Ta 7Cr
AGING TEMP 700°C
SOLUTION
TREATED
1
10
100
1000
AGING TIME, MIN.
XBL 737-6447

Fig. 6.

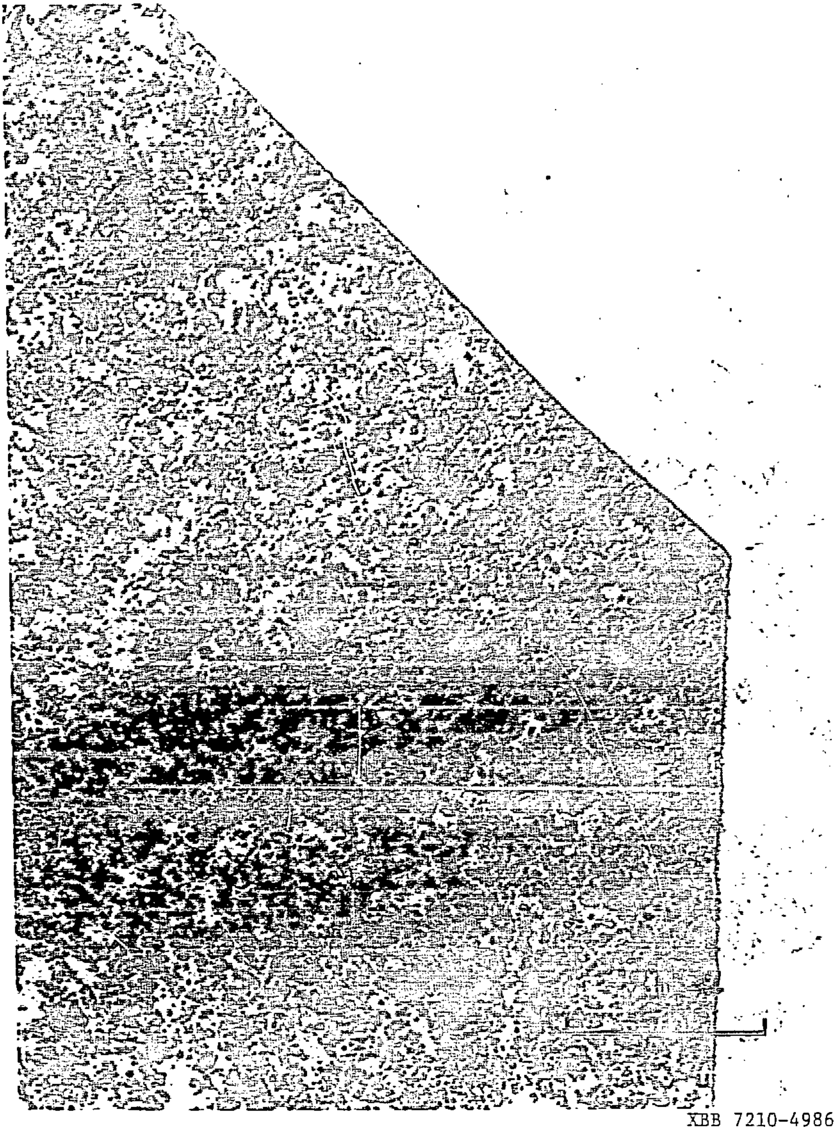

XBB 7210-4986

Fig. 7.

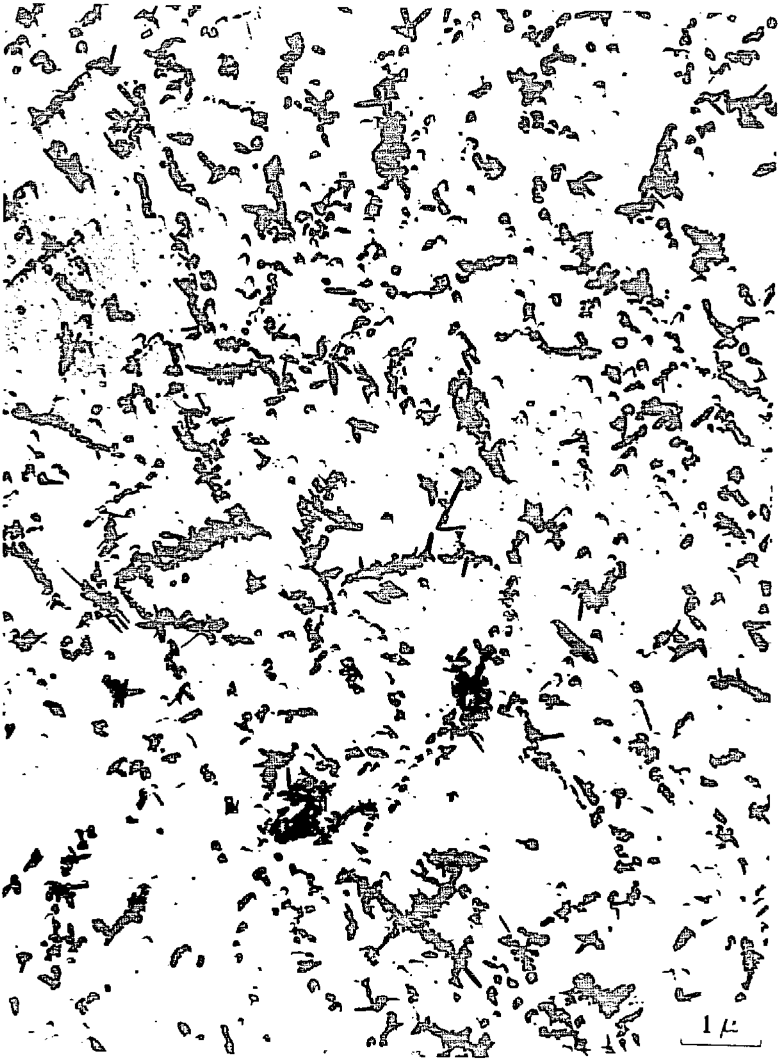

XBB 738-5042

Fig. 8.

XBB 7210-4985

Fig. 9.

XBB 738-5043

Fig. 10.

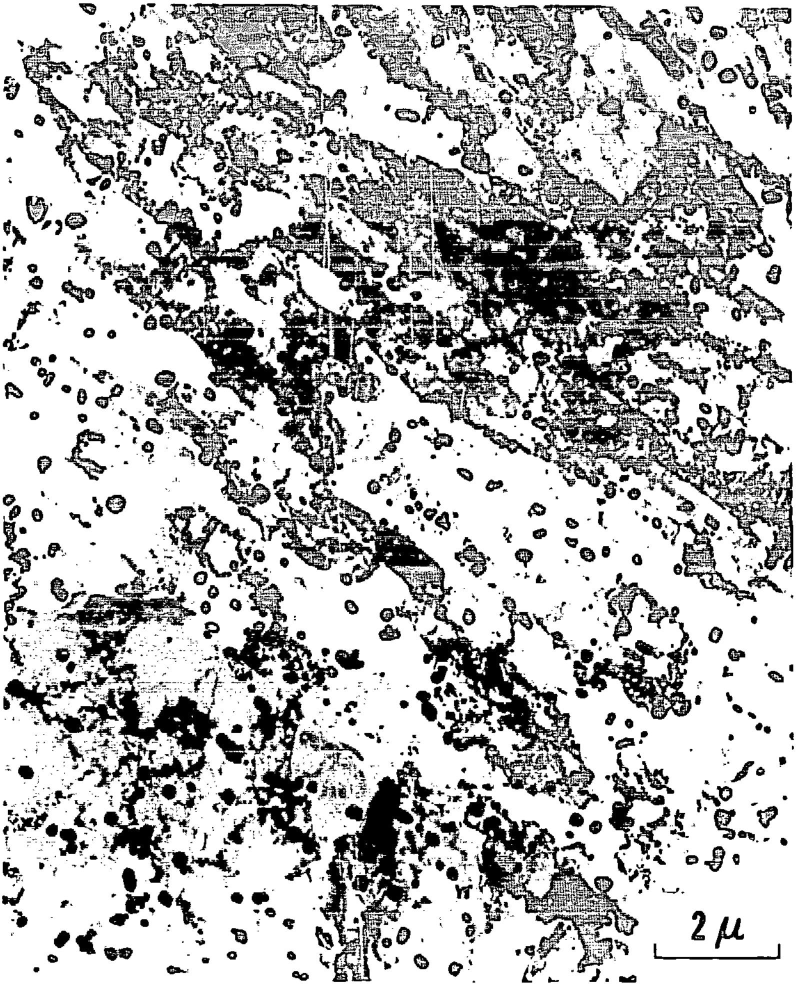

XBB 738-5041

Fig. 11.

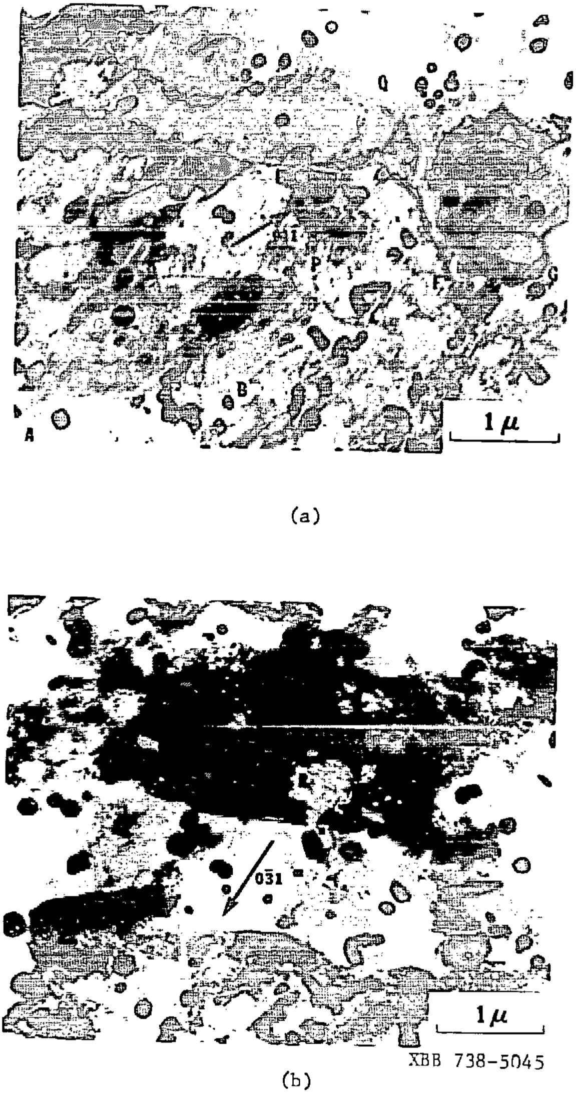

(a)

XBB 738-5045

(b)

Fig. 12.

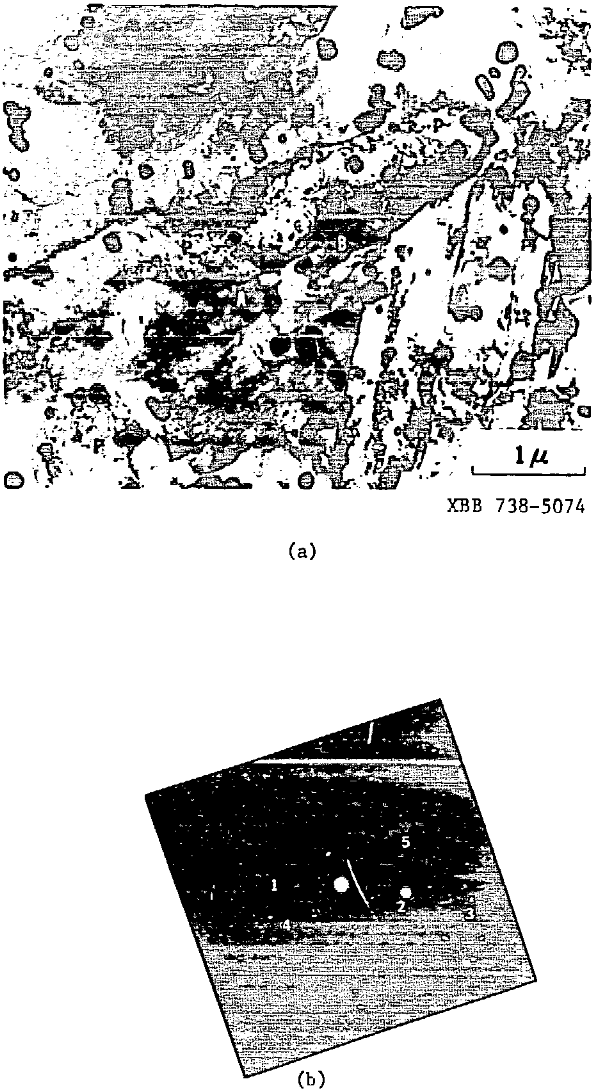

XBB 738-5074

(a)

(b)

Fig. 13.

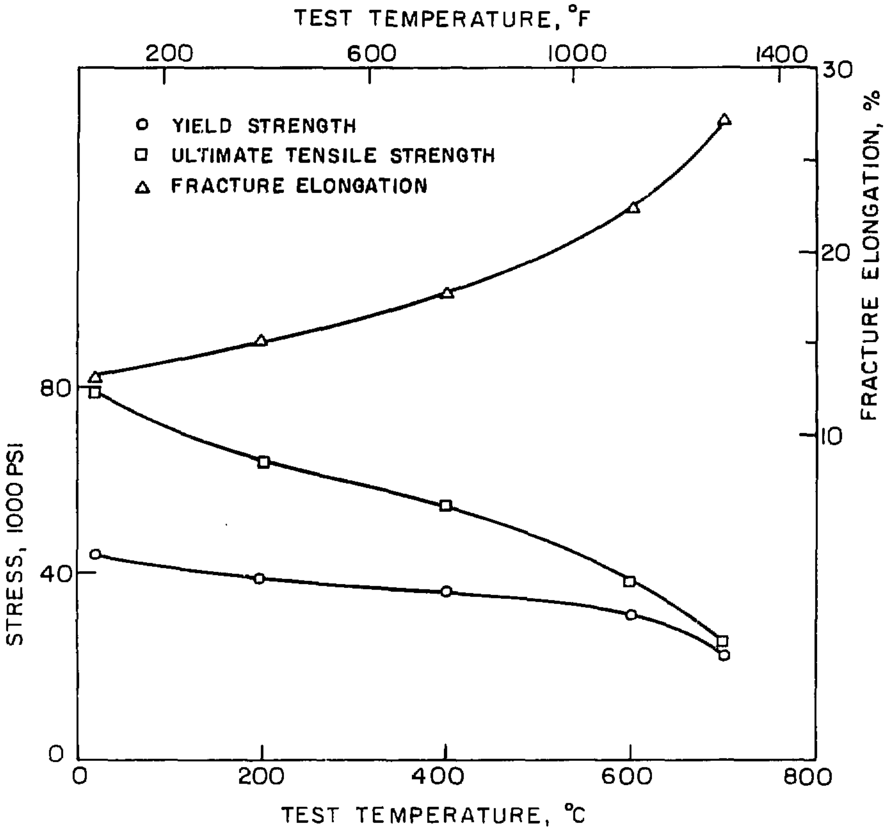

XBL737-6448

Fig. 14.

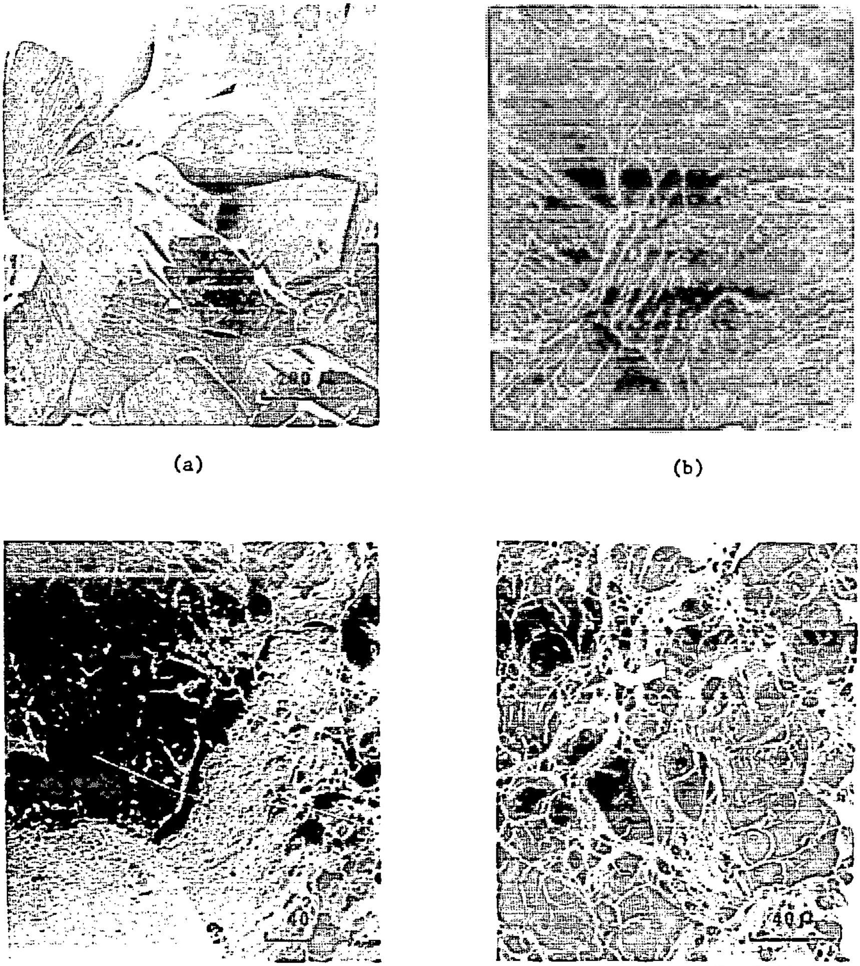

(a) (b) (c) (d)

XBB 7210-4992

Fig. 15.

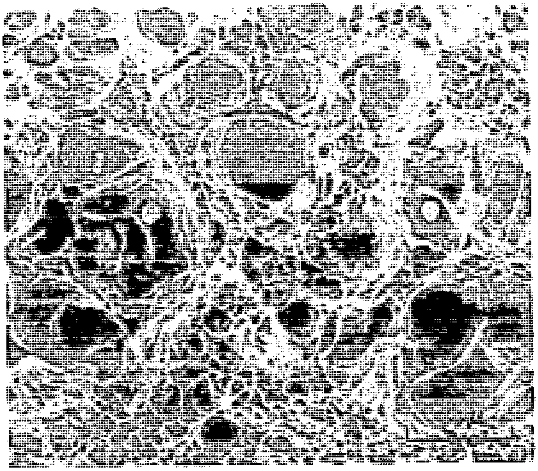

(a)

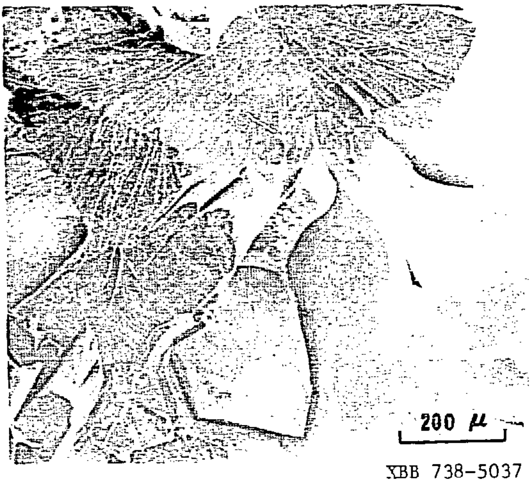

XBB 738-5037

(b)

Fig. 16.

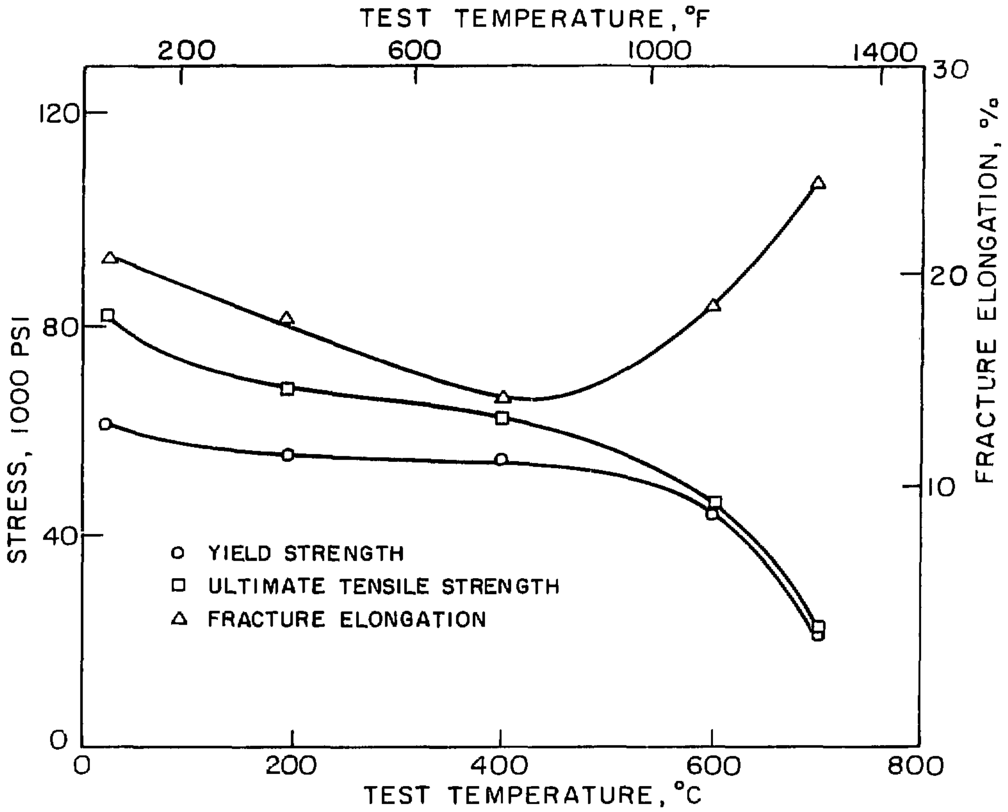

XBL737-6449

Fig. 17.

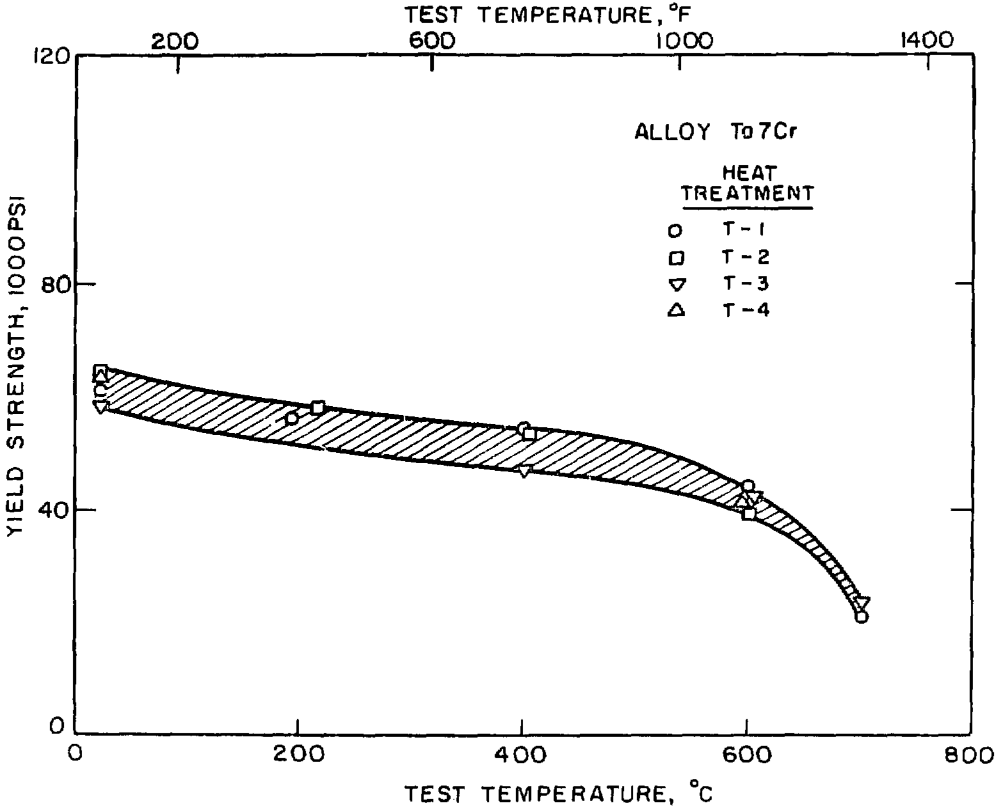

XBL737-6450

Fig. 18.

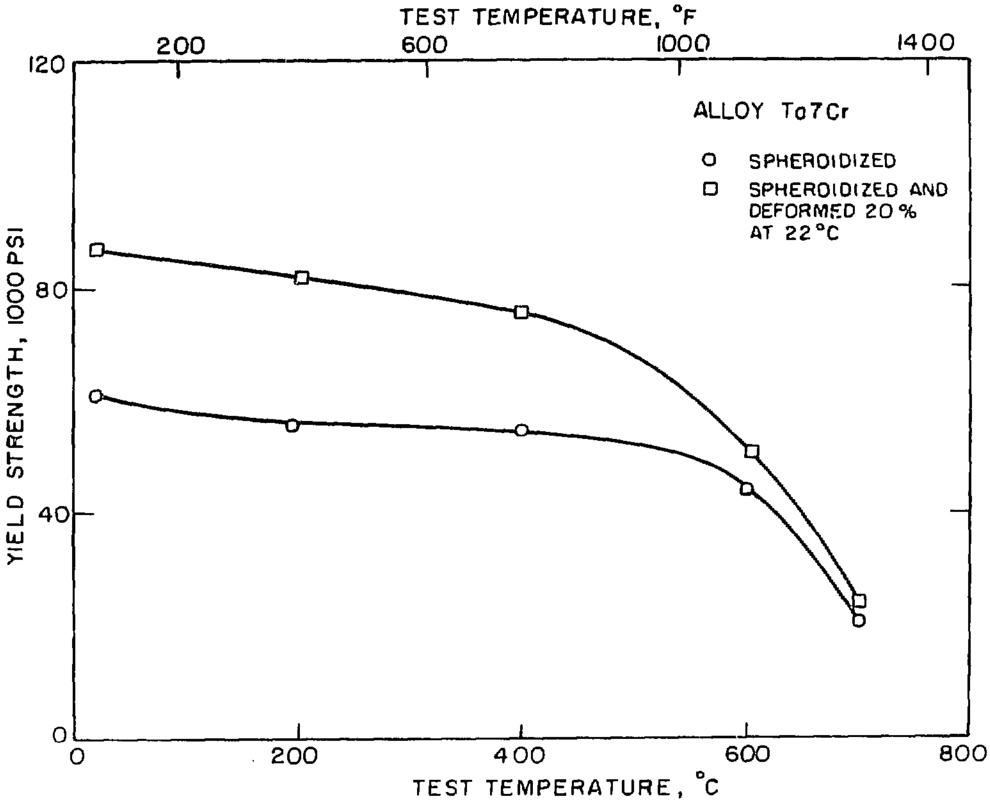

XBL737-6451

FIG. 19.

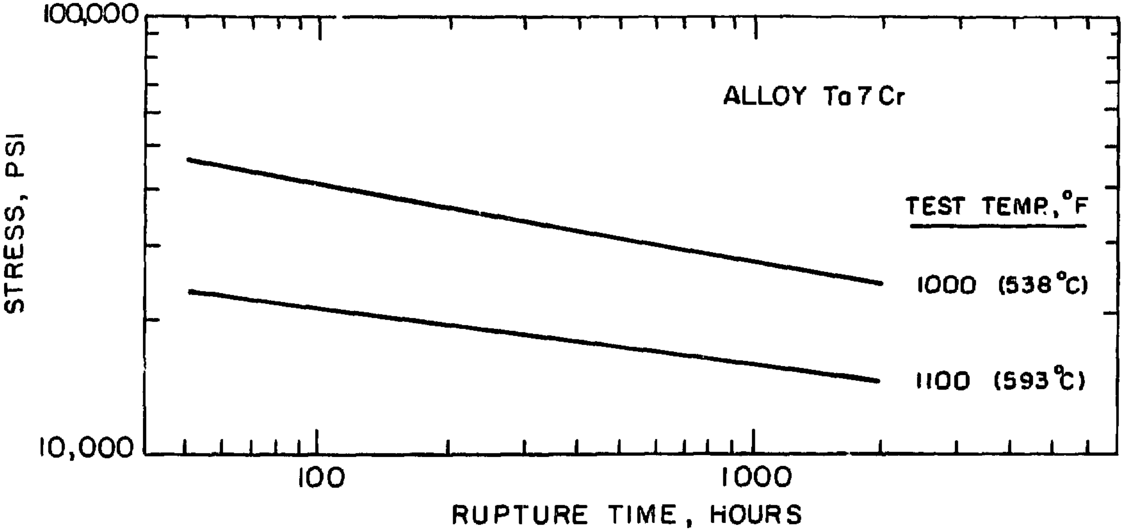

XBL 738-1777

Fig. 20.

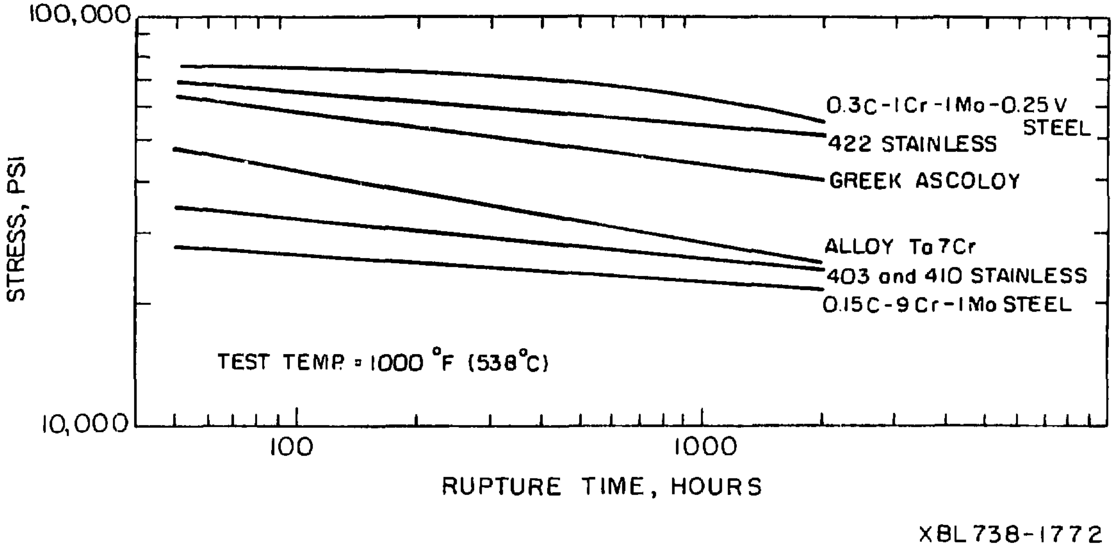
100,000
10,000
STRESS, PSI
100
1000
RUPTURE TIME, HOURS
0.3C-1Cr-1Mo-0.25V STEEL
422 STAINLESS
GREEK ASCOLOY
ALLOY To 7Cr
403 and 410 STAINLESS
0.15C-9Cr-1Mo STEEL
TEST TEMP = 1000 °F (538°C)
XBL 738-1772

Fig. 21.

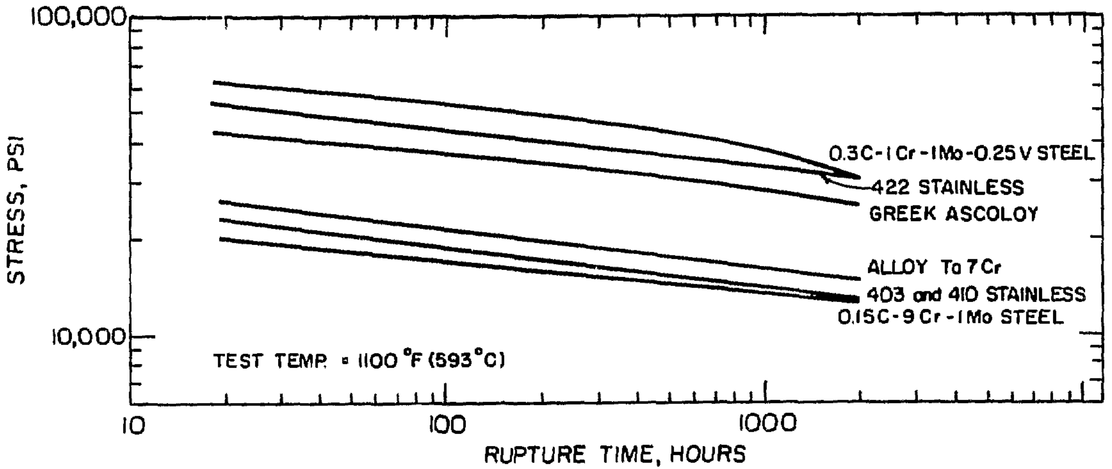

XBL 738-1774

Fig. 22.

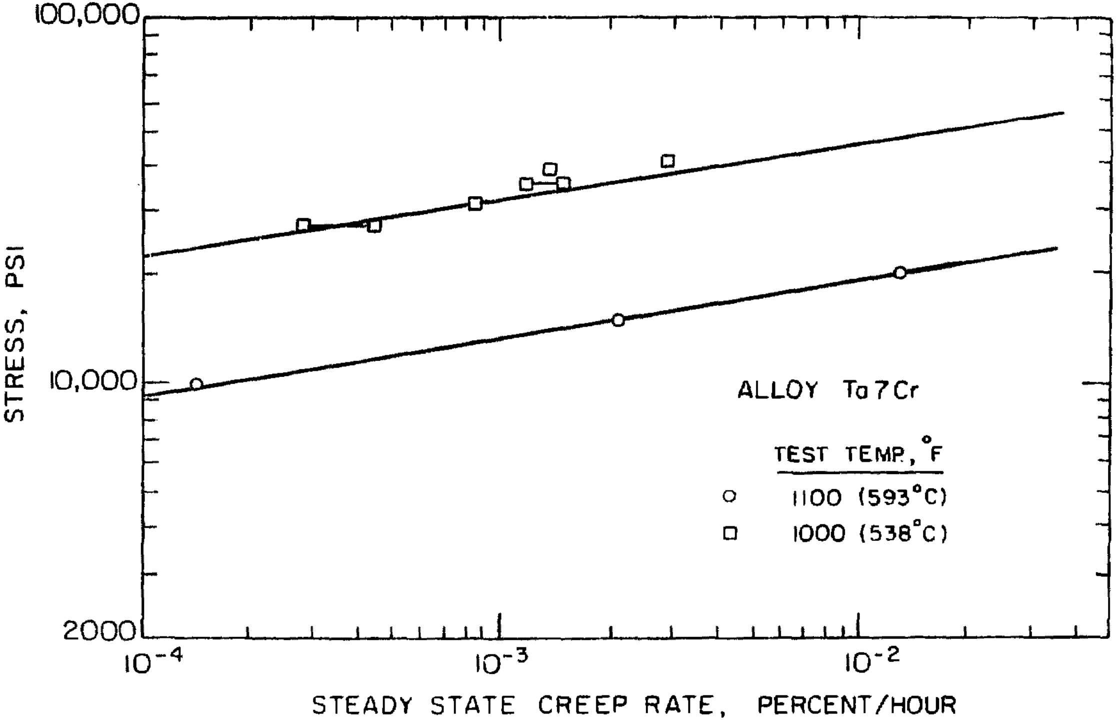

XBL738-1776

Fig. 23.

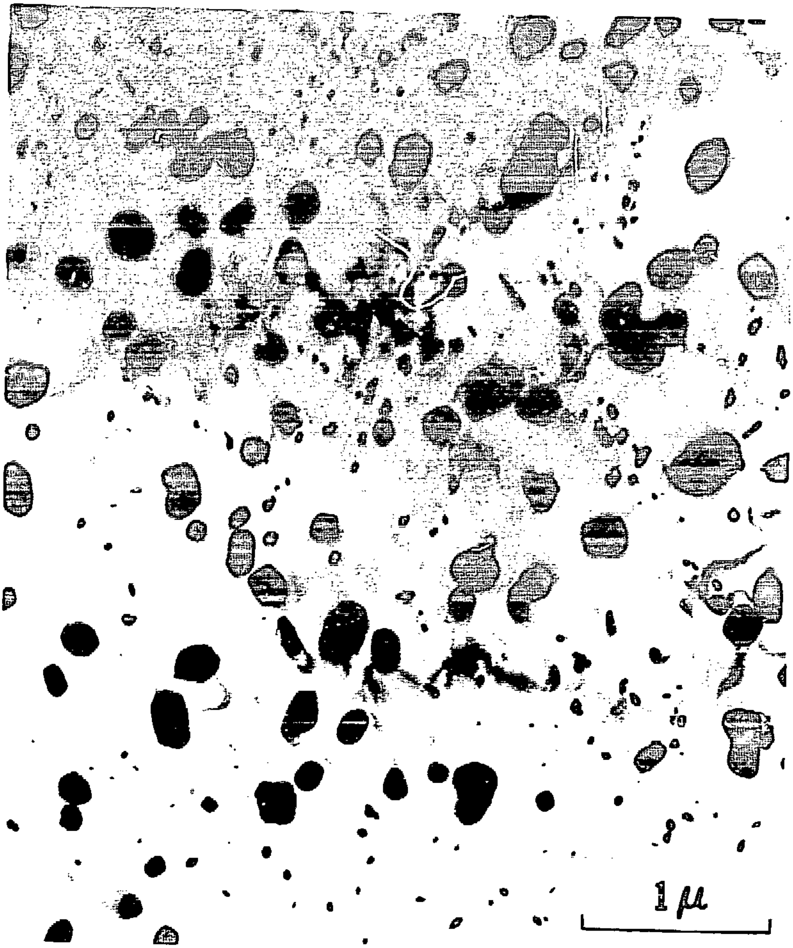

XBB 738-5039

Fig. 24.

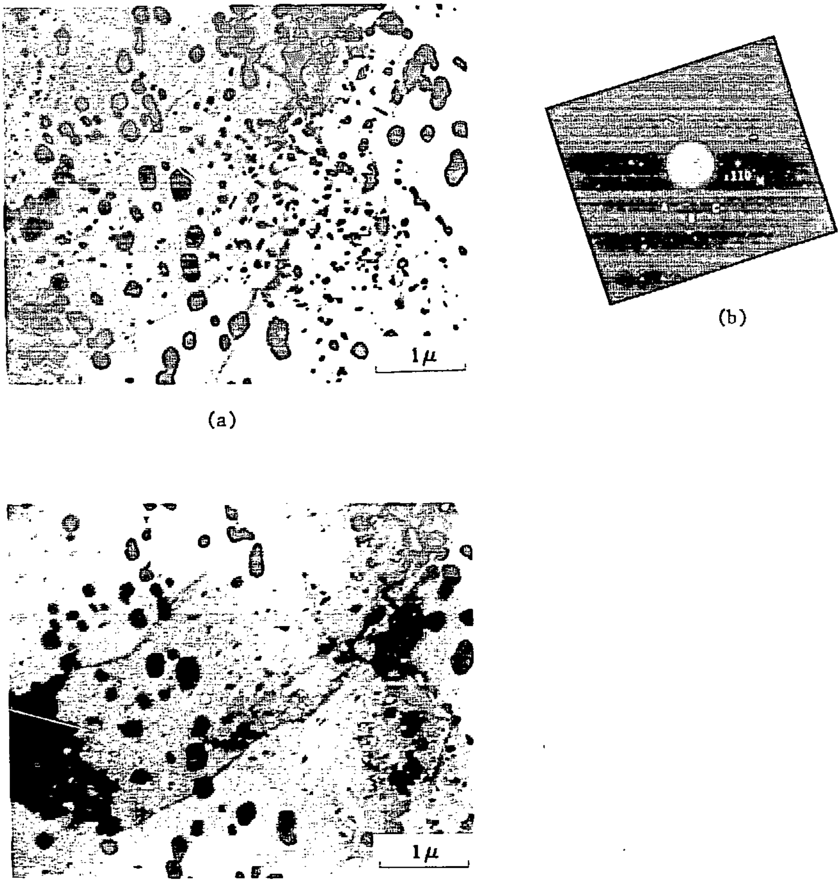

(a)

(b)

XBB 738-5078

(c)

Fig. 25.

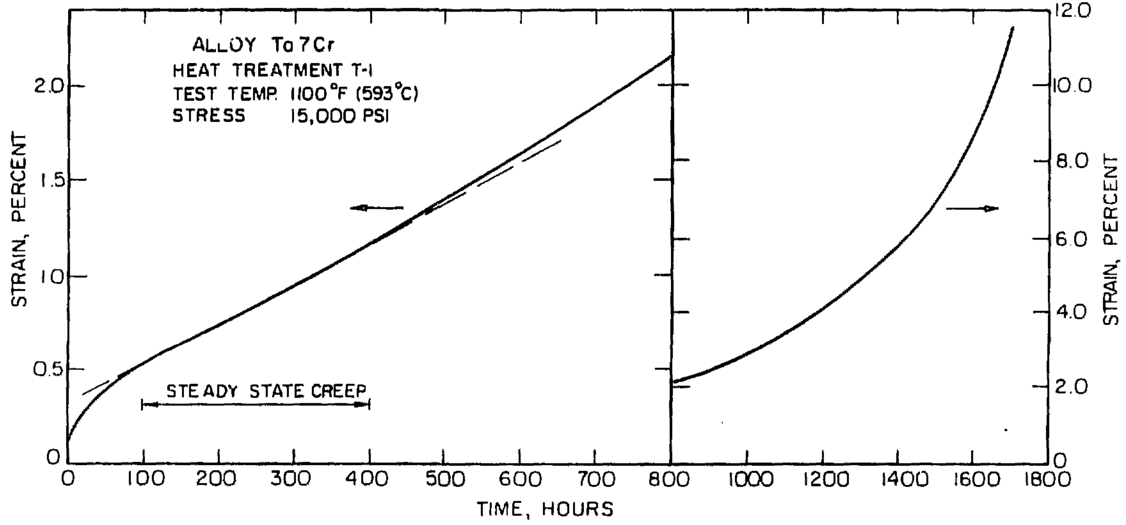

XBL 738-1748

Fig. 26.

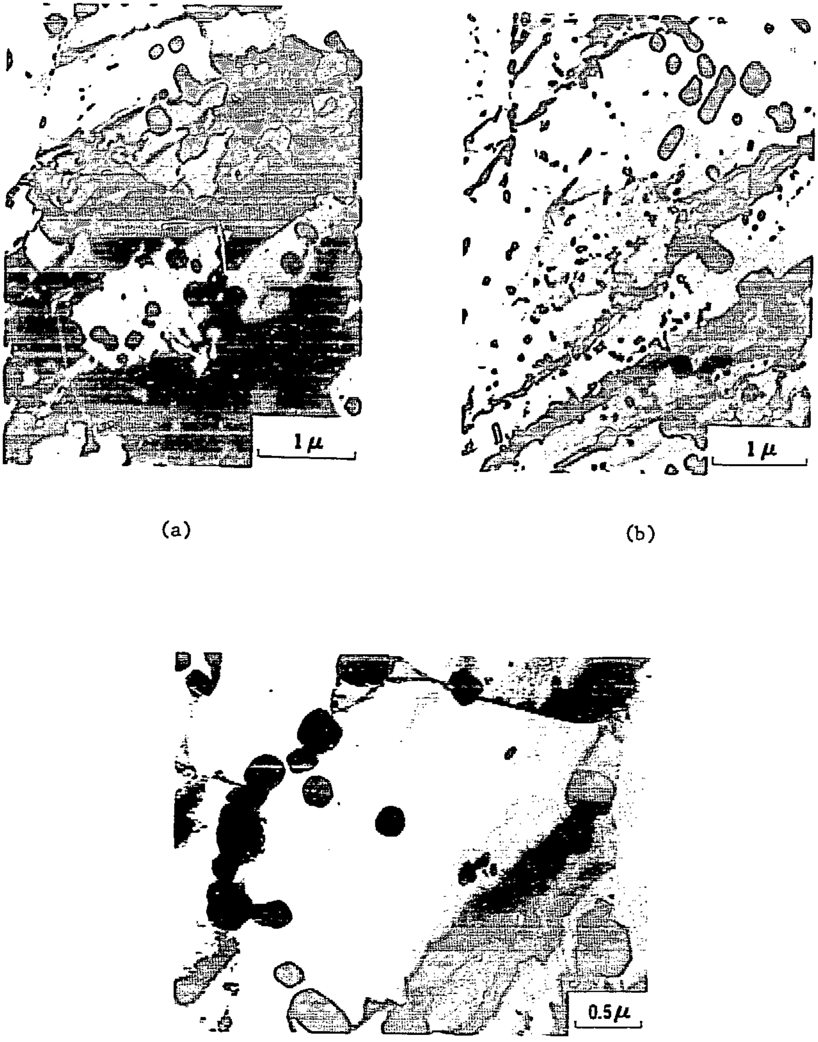

(a)

(b)

(c)

XBB 738-5050

Fig. 27.

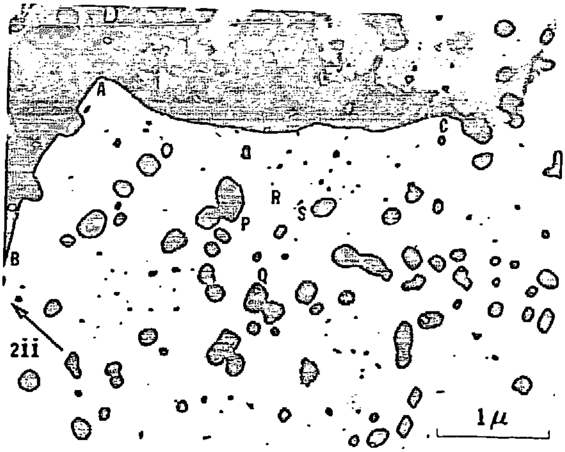

Fig. 28.

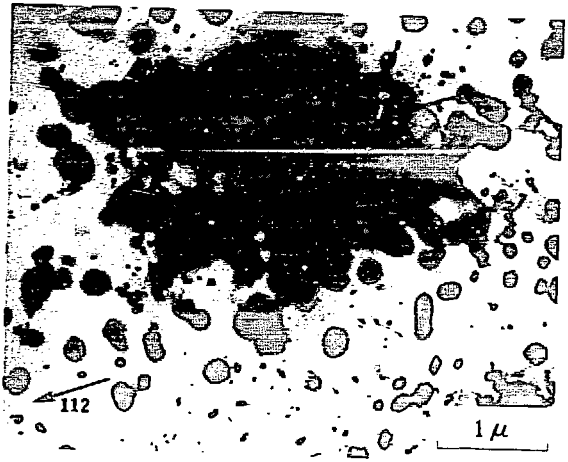

XBB 738-5049

Fig. 29.

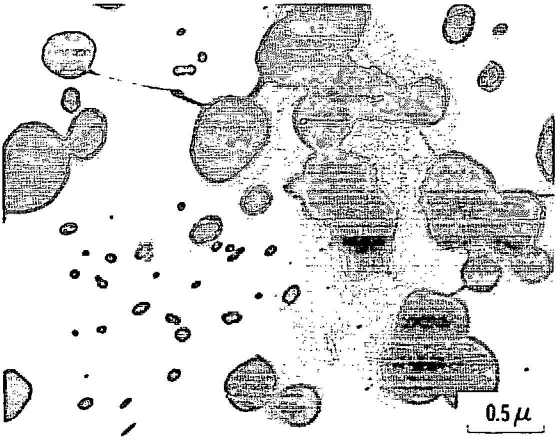

Fig. 30.

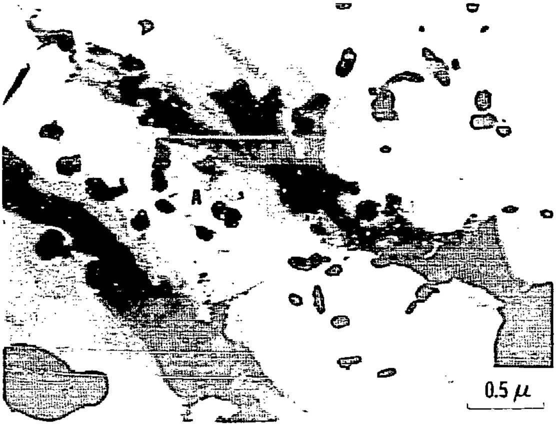

XBB 738-5048

Fig. 31.

XBB 738-5040

Fig. 32.

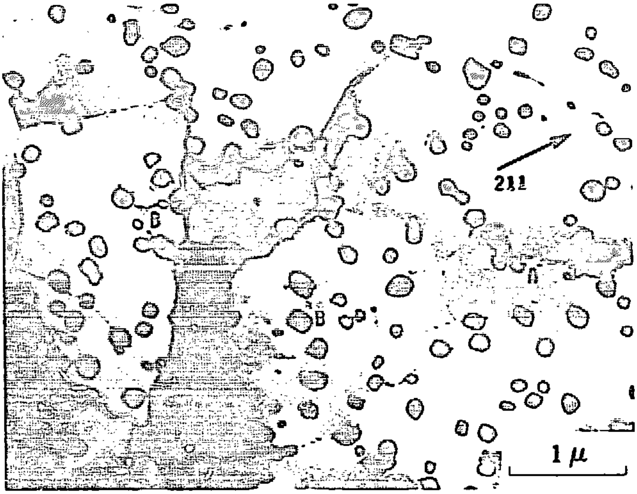

XBB 738-5038

(a)

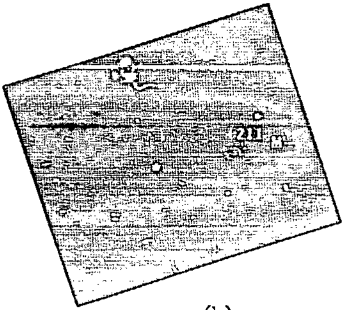

(b)

Fig. 33.

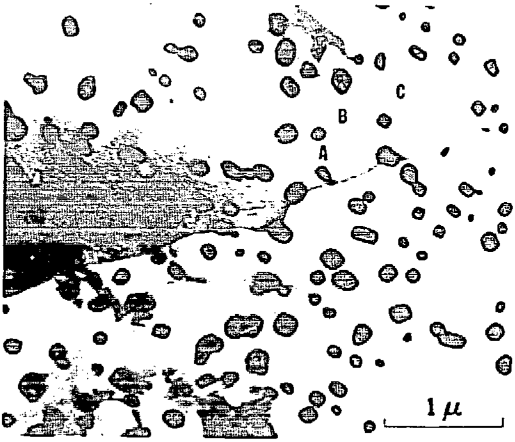

Fig. 34.

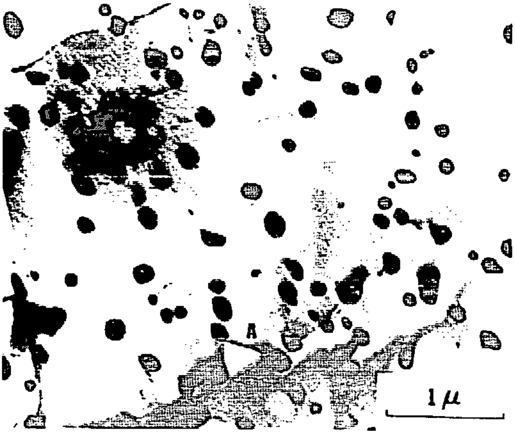

XBB 738-5047

Fig. 35.

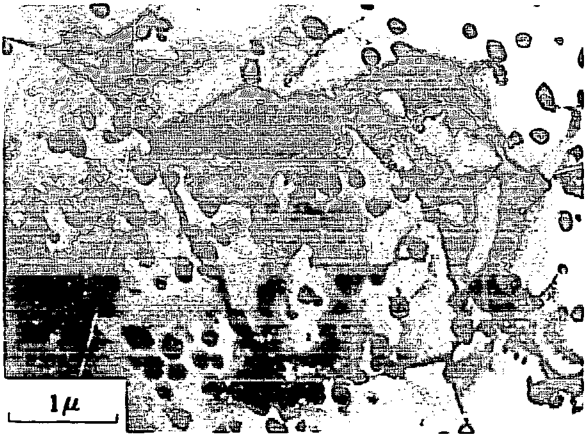

Fig. 36.

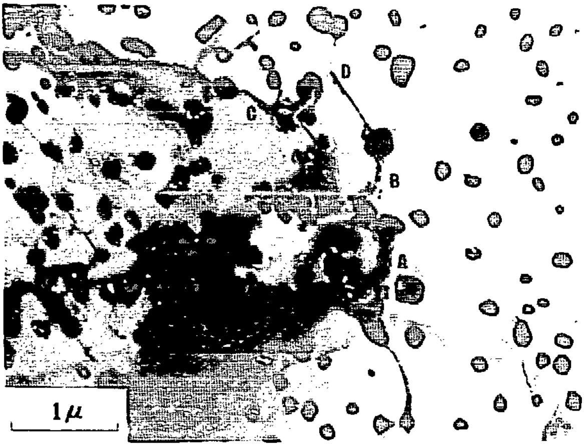

XBB 738-5046

Fig. 37.

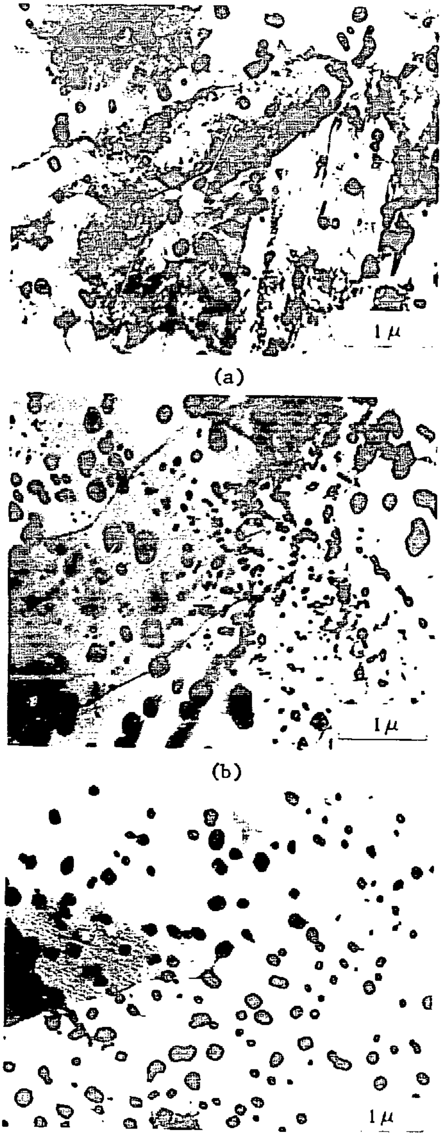

(a)

(b)

(c)

XBB 738-5051

Fig. 38.

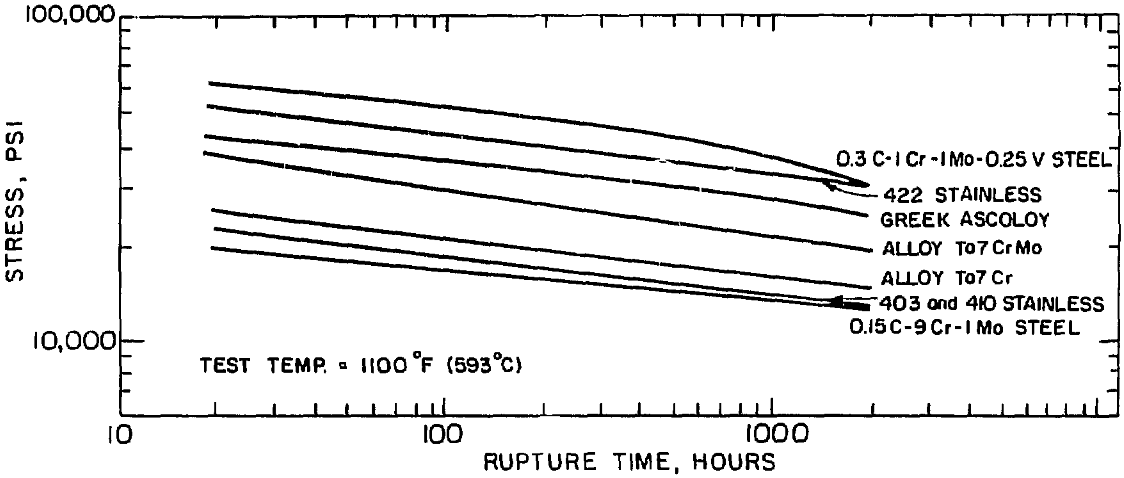

XBL738-1773

Fig. 39.

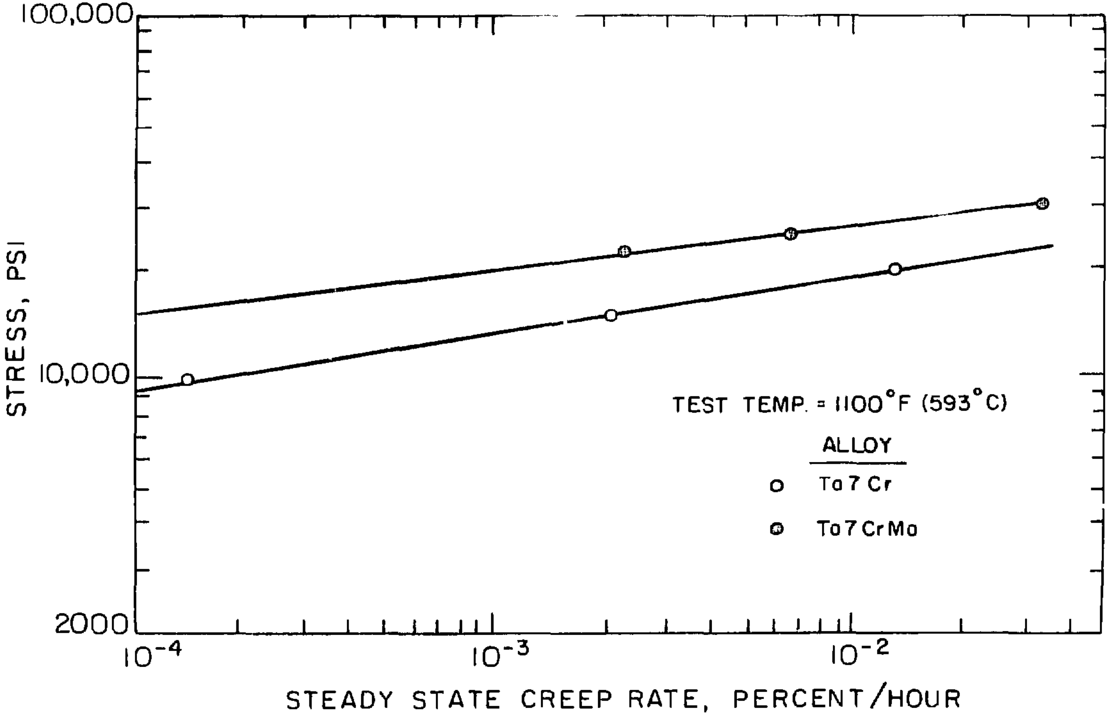

XBL738-1775

Fig. 40.

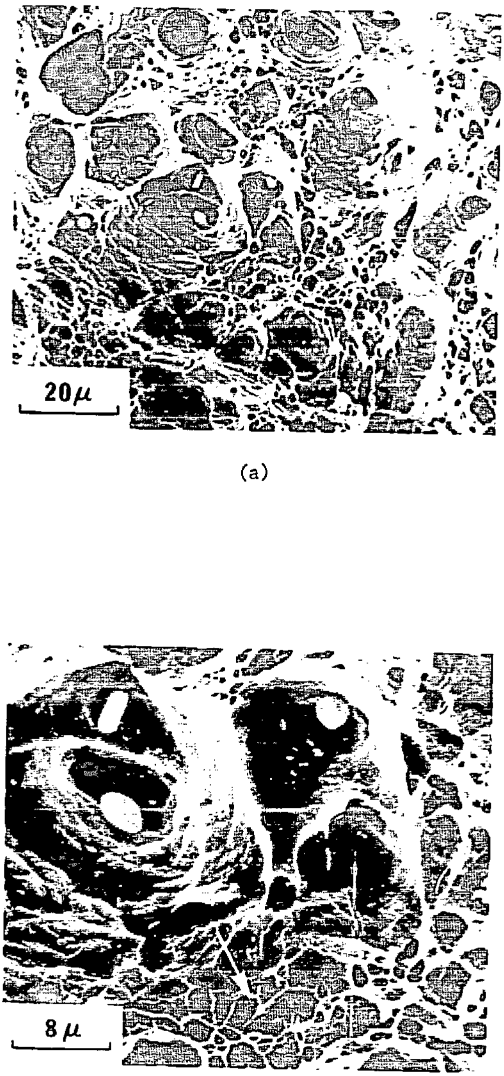

(a)

XBB 738-5075

(b)

Fig. 41.

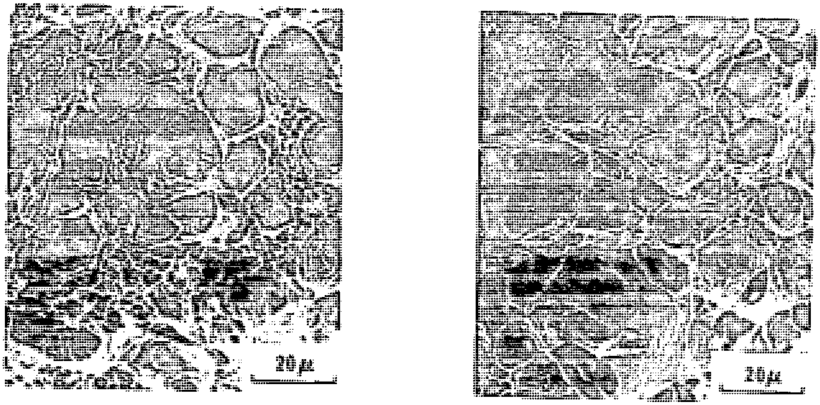

(a) 42,500 PSI
RUPTURE TIME 3.5 HRS

(b) 40,000 PSI
RUPTURE TIME 140 HRS

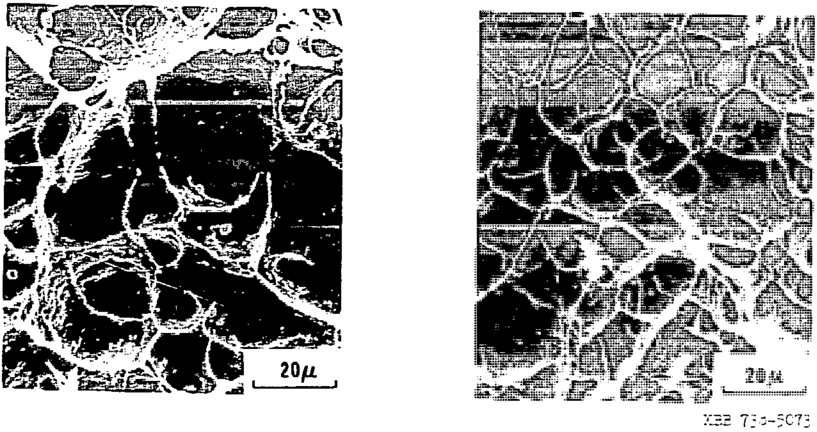

(c) 38,000 PSI
RUPTURE TIME 185 HRS

(d) 27,000 PSI
RUPTURE TIME 1181 HRS

Fig. 42.

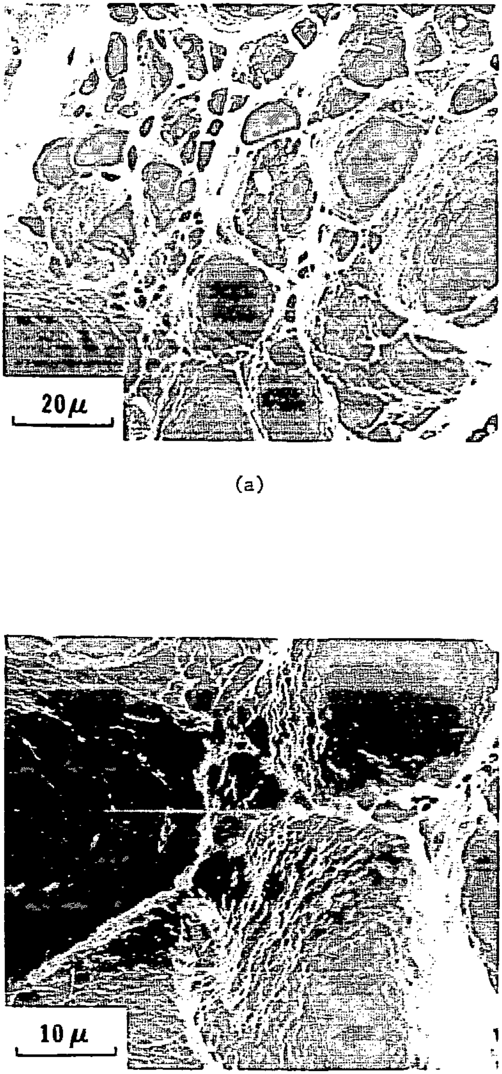

(a)

(b)

XBB 738-5072

Fig. 43

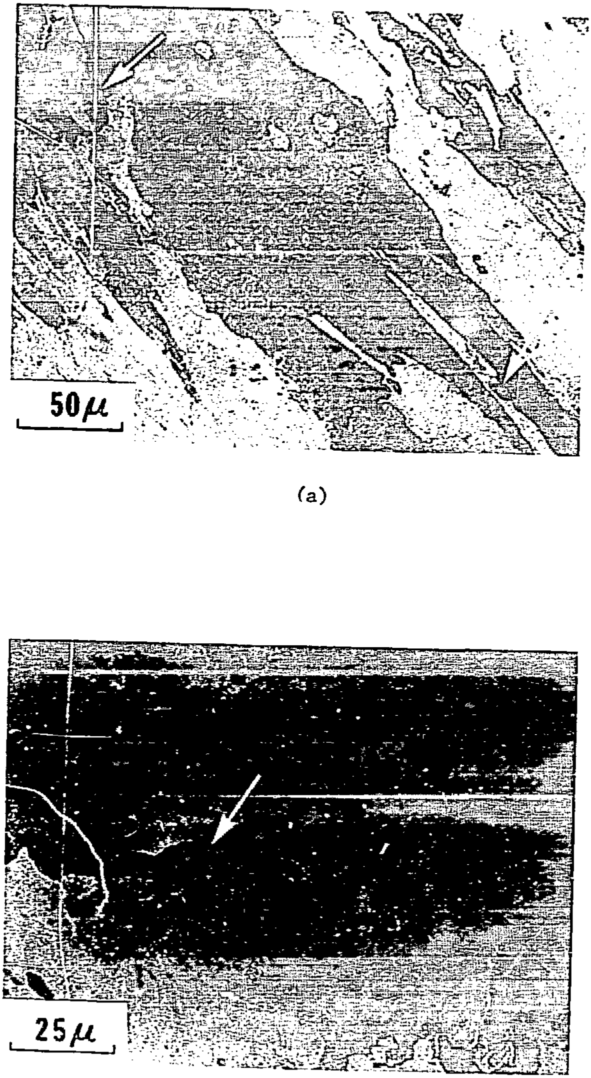

(a)

(b)

XBB 738-5076

Fig. 44.

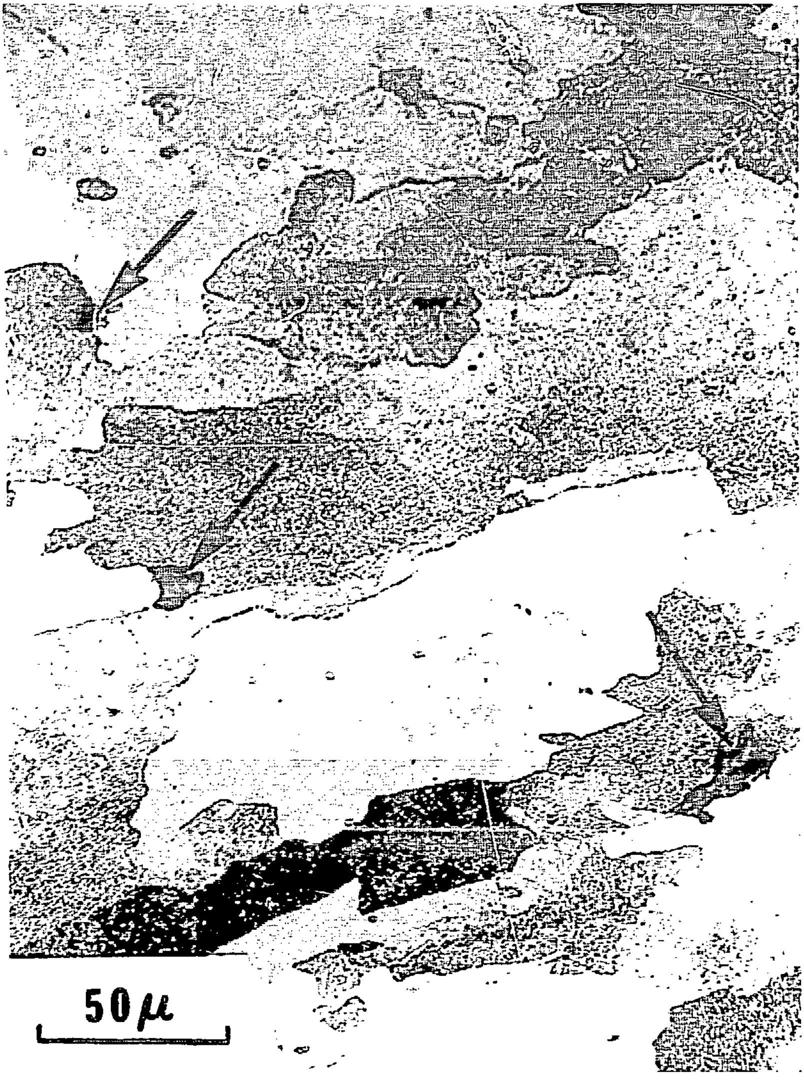

XBB 738-5077

Fig. 45.

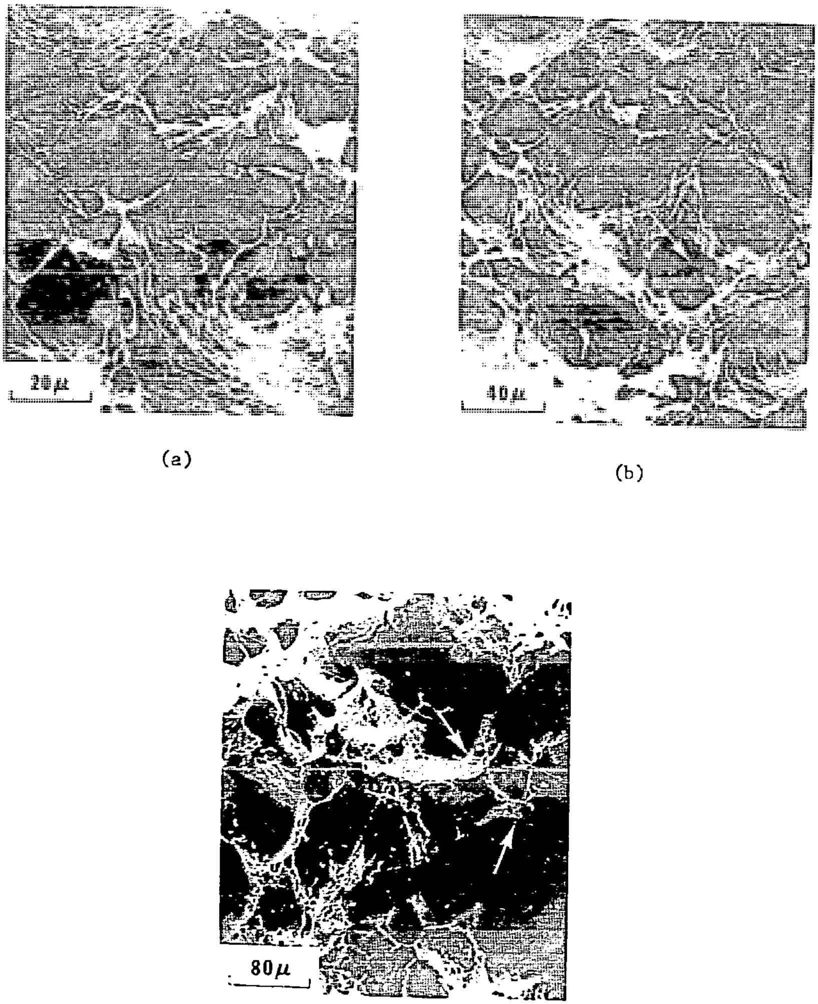

(a)

(b)

(c)

XBB 738-5044

Fig. 46.